

11. INTERSTITIAL WATER CHEMISTRY—MAJOR CONSTITUENTS¹

Joris M. Gieskes,² Gerard Blanc,³ Peter Vrolijk,^{4,5} Henry Elderfield,⁶ and Ross Barnes⁷

ABSTRACT

Major-element compositions (Cl^- , SO_4^{2-} , Ca^{2+} , Mg^{2+} , Li^+ , K^+ , Na^+ , Sr^{2+}) of interstitial waters obtained from sediment cores along the ODP Leg 110 transect across the Northern Barbados accretionary prism have shown that a complex set of geochemical processes are of importance in this area. In the volcanic ash-rich Pleistocene-Pliocene sediments, alteration reactions involving volcanic ash lead to depletions of Mg^{2+} and K^+ . This process is confirmed by the much lower than contemporaneous seawater values of the $^{87}\text{Sr}/^{86}\text{Sr}$ ratios of dissolved strontium. In the deeper sediments recovered below the zone of décollement (Sites 671 and 672) large increases in Ca^{2+} and gradual decreases in Mg^{2+} , Na^+ , and $\delta^{18}\text{O}$ (H_2O) indicate a potential contribution to the interstitial water chemistry by exchange with underlying basement rocks. This process has been hard to confirm because the drill holes were terminated well short of reaching basement. However, the concentration gradient pattern is consistent with observations in a large number of DSDP drill holes. Finally, but most importantly, low Cl^- concentrations in the décollement zone and underlying sand layers, as well as in fault zones at Sites 673 and 674, indicate dilution of interstitial waters. The potential origins of the low Cl^- concentrations are discussed, though we are not able to distinguish any mechanism in particular. Our evidence supports the concept of water migration along the décollement and through the underlying sandstones as well as along recent fault zones in the accretionary complex. Interstitial water concentration depth profiles are affected by faulting, thrusting, and overturn processes in the accretionary prism. These processes have caused a diminished diffusive exchange with the overlying ocean, thus explaining increased depletions in Mg^{2+} and SO_4^{2-} in sites farther onto the accretionary prism.

INTRODUCTION

Subduction zones are among the most dynamic tectonic environments on earth. In these zones water-rich sediments evolve into highly deformed rocks of negligible porosity by the time of their exposure at the surface (Bray and Karig, 1985). This porosity reduction requires large-scale fluid expulsion, which must occur sometime during underthrusting and deformation. Leg 78A of the Deep Sea Drilling Project (Biju-Duval, Moore et al., 1984) and Leg 110 of the Ocean Drilling Project (Moore, Mascle, Taylor, et al., 1987) were specifically designed to investigate the structural, hydrologic, and diagenetic processes at shallow levels in accretionary complexes. The focus of this paper is on the geochemistry of the interstitial fluids.

The northern Barbados Ridge complex (Fig. 1) became the focus of subduction zone drilling because the sedimentary cover of the incoming oceanic crust is less than 800 m thick and, consequently, the décollement zone and related thrust faults occur at relatively shallow depths below the seafloor. Biostratigraphic observations during Deep Sea Drilling Project (DSDP) Leg 78A (Biju-Duval, Moore, et al., 1984) documented thrust faulting in the accretionary wedge. In addition there were indications of high fluid pressures in the décollement zone, but this major fault zone was not penetrated. The décollement zone consists of siliceous clays and muds, which are characterized by higher po-

rosities than those of the surrounding sediments. The physical properties of such sediments cause this zone to serve as an excellent shear zone, below which relatively undeformed sediments are subducted below strongly deformed accreting sediments (Moore, Mascle, et al., 1987). Penetration of the décollement zone was achieved during ODP Leg 110 at Site 671. Extensive shipboard analyses included studies of heat flow, physical properties, structural geology, and biostratigraphy, as well as of the chemistry of interstitial waters, gases, and organic carbon.

During Leg 110 a total of six drill sites were occupied (Fig. 1). Prior to this drilling leg interstitial waters were obtained from three sites drilled during Leg 78A of the Deep Sea Drilling Project (Gieskes et al., 1984). In this report we discuss the shipboard data on the inorganic major element composition of dissolved salts in the interstitial waters as well as data obtained in two of our home laboratories (J.M.G. and H. E.). Stable isotope geochemical data on the interstitial waters are presented elsewhere in this volume by P. Vrolijk and co-workers.

METHODS AND RESULTS

The interstitial water program carried out during Leg 110 is principally based on analyses of samples obtained by routine squeezing techniques (Manheim and Sayles, 1974) using stainless steel squeezers, operated at pressures of about 2000–3000 psi (140–210 $\text{kg} \cdot \text{cm}^{-2}$). In addition a few samples were obtained by means of an *in-situ* sampler (Barnes, 1988; Barnes et al., 1979), but generally our attempts at consistent *in-situ* sampling were thwarted by the nature of the sediments.

Shipboard analyses for pH, alkalinity, S, Cl^- , Ca^{2+} , Mg^{2+} , SO_4^{2-} , H_4SiO_4 , and NH_4^+ were carried out by means of methods described by Gieskes and Peretsman (1986). For Cl^- both an indicator method and an electrometric method (G. Blanc) were used, leading to identical results. The analyses for Li^+ and Sr^{2+} were made by means of flame atomic absorption spectrometry. K^+ was analyzed by emission spectroscopy. $^{87}\text{Sr}/^{86}\text{Sr}$ ratios (H. Elderfield) were obtained from mass spectrometry. Br^- analyses were carried out by a colorimetric technique described by Presley (1971). All concentrations are expressed in molar concentra-

¹ Moore, J. C., Mascle, A., et al., 1990. *Proc. ODP, Sci. Results*, 110; College Station, TX (Ocean Drilling Program).

² Scripps Institution of Oceanography, La Jolla, CA 92093.

³ Centre de Géochimie de Surface Université Louis Pasteur F-67084 Strassbourg, France.

⁴ Department of Geological Sciences, University of Michigan, Ann Arbor, MI 48109-1063.

⁵ Current address: Exxon Production Research PO Box 2189 Houston, TX 77252-2189.

⁶ Department of Earth Sciences, University of Cambridge, Cambridge, CB2 3EQ, U.K.

⁷ Rosario Geoscience Associates, Anacortes, WA 98221.

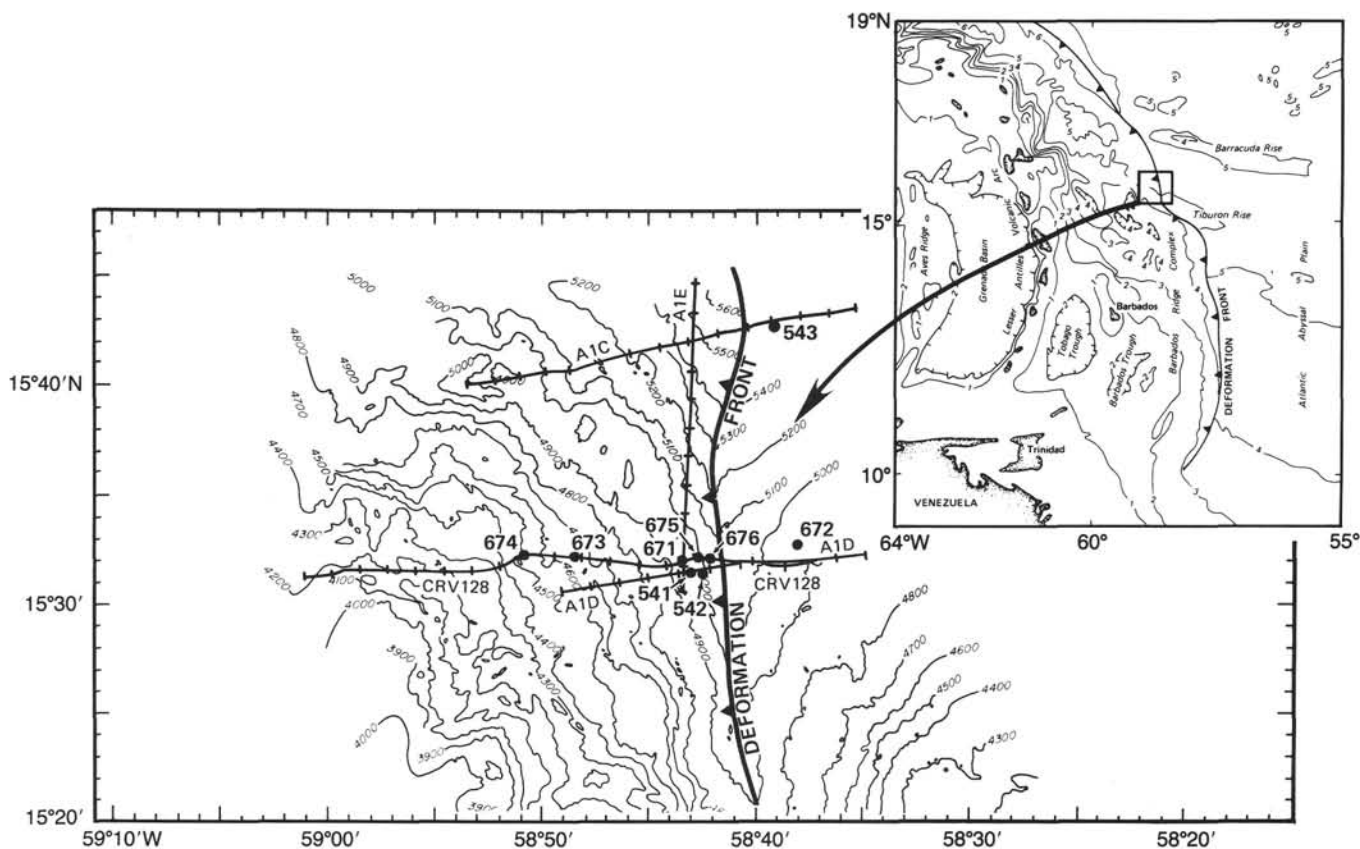


Figure 1. Map of study areas of DSDP Leg 78A and ODP Leg 110. Bathymetry in meters.

tions on a volumetric basis ($\text{mM} = \text{millimol} \cdot \text{dm}^{-3}$; $\mu\text{M} = \text{micromol} \cdot \text{dm}^{-3}$).

Accuracies of the analytical data generally are better than 2%, but artifacts of squeezing may cause systematic offsets in the data (usually less than 5%). However, concentration-depth trends are not significantly affected (Gieskes, 1974; Manheim and Sayles, 1974). Large changes in chloride concentrations were observed, which led us to investigate the validity of our methodologies, especially because of the important implications of decreases in chloride observed in this study.

Validity of Chloride Concentrations

To ascertain that observed variations in chloride concentrations were not an artefact of the pore-water extraction procedures, we directed our attention to possible pressure effects during the hydraulic squeezing process.

Manheim (1974) has reviewed the various methods of pore-water extraction with special emphasis on methods using hydraulic squeezers. He cites evidence collected by himself (Manheim, 1966) and by Shiskina (1966) that no membrane filtration process or removal of adsorbed waters on clays occurs at pressures of 580–12000 psi ($39\text{--}820 \text{ kg} \cdot \text{cm}^{-2}$); i.e., over a pressure range much larger than that used in this study (2000–3000 psi). Sayles (1970), however, suggested from his experiments on a NaCl ($29 \text{ g} \cdot \text{kg}^{-1}$)-saturated clay (low carbonate) that small effects could occur at pressures in excess of 2400 psi, but only if very small quantities ($< 1 \text{ cm}^3$) of water were recovered.

Notwithstanding our conviction that our observations on decreased chloride concentrations are not the result of a sampling artifact, we carried out a series of experiments in which interstitial waters were expressed from the sediments at different pres-

ures and in a sequential fashion (often in 3- to 4- cm^3 aliquots). Sediment samples at Site 674 were chosen for this purpose. The results are given in Table 1 and in Figure 2. Many of the results did show that usually the first water obtained had higher sulfate contents, particularly in brecciated samples that may have been exposed to surface seawater that is used as drilling fluid. As observed in split cores, often only small pieces of undisturbed native sediment occur in a matrix of disturbed material. Thus, even though attempts were made to squeeze the best samples, some contamination is unavoidable. A study of the SO_4^{2-} concentration-depth profile, however, suggests that these contamination problems are relatively minor except for samples from about 125 mbsf, 190 mbsf, and 305 mbsf. At about 395 mbsf we squeezed some mud peelings knowing that they should be contaminated with seawater. This shows quite clearly in anomalous data in SO_4^{2-} , Cl^- , and Mg^{2+} , but less in Ca^{2+} . A precise dilution effect, however, cannot be expected because of potential ion exchange effects introduced by the drilling fluid seawater of different Cl^- (and Na^+) content. Often lower Cl^- concentrations appear to accompany the lower SO_4^{2-} concentrations, but we prefer to interpret this in terms of a more pristine sample, rather than in terms of a dilution effect caused by membrane filtration. In any case, Cl^- differences are usually well within 2%, which is relatively small compared to the overall observed changes in Cl^- with depth (about 30%). Effects on Ca^{2+} and Mg^{2+} below the sediment water interface indicate again that the Cl^- decrease at about 20 mbsf cannot be the result of seawater contamination. Indeed, as will be discussed later for Site 674, the Cl^- minimum coincides with a temperature anomaly, which suggests advective fluid flow in these sediment layers (Fisher and Hounslow, this volume). We conclude that the observed

Table 1. Consecutive squeeze results, Hole 674A.

Core, section interval, cm	Pressure, (PSI × 10 ²)	Depth (mbsf)	Ca (mM)	Mg (mM)	SO ₄ (mM)	Cl (mM)
1-3, 145-150	20-30	4.5	11.5	50.1	24.3	546
2-6, 145-150	20-30	15.5	15.8	46.4	24.0	543
3-5, 145-150	20-30	23.5	21.2	40.8	20.0	537
4-3, 145-150	20-30	30	25.2	38.4	18.0	518
5-4, 145-150	20-30	40.5	29.8	27.5	15.5	569
7-2, 145-150	20-30	57	33.3	22.3	13.0	565
9-6, 140-150	20(1)	82	37.6	19.2	11.2	571
	20(2)				10.8	560
	30(1)		37.7	19.6	11.1	559
						558
						553
	30(3)		37.5	20.0		561
12-3, 140-150	20(1)A	105	38.9	13.2	7.4	560
	20(1)B					558
	30(2)A		38.6	13.9	7.8	558
	30(2)B					559
	30(3)A		38.8	14.3	7.2	542
15-2, 140-150	20(1)A	132	39.7	14.2		545
	20(1)B					544
	30(2)A		40.6	13.3		540
	30(2)B					548
	30(3)A		40.9	11.6		543
	30(3)B		40.9	12.2		546
	30(4)A		40.8	11.5		542
	30(4)B		40.6	12.9		535
18-5, 140-150	20(1)	165				530
	30(2)		46.2	4.9		532
	30(3)					549
21-3, 140-150	20(1)A	190	44.4	6.3	6.0	528
	20(1)B		45.6	7.5	8.1	549
	30(2)A		44.4	5.5	5.1	529
	30(2)B		44.4	6.1	6.0	547
	30(3)A		45.0	4.7	4.1	527
	30(3)B		44.6	5.1	5.0	512
24-5, 140-150	20(1)A	220	44.6	6.7	4.0	516
	20(1)B		44.1	5.6	4.2	503
	30(2)A		43.2	4.9	2.8	501
	30(2)B		42.7	5.0	2.8	500
	30(3)A					489
27-5, 140-150	20(1) 1 ml	250	39.9	10.8		481
	30(2) 4 ml		38.8	9.5	1.8	507
30-3, 140-150	20(1)	275	41.2	12.9	1.6	508
	30(2)		40.2	11.7	0.9	479
33-5, 140-150	20(1) 2 ml	308	38.7	12.8	4.6	455
	30(2) 5 ml		35.7	11.6	3.8	477
36-5, 140-150	20(1)	336	38.2	8.6	2.3	469
	30(2)		36.7	8.8	2.1	465
	30(3)		35.9	8.8	1.7	510
39-5, 140-150	20(1)A	365	39.8	9.7	1.8	505
	20(1)B		40.0	9.9	1.0	504
	30(2)A		38.9	9.4	1.0	500
	30(2)B		39.0	9.7	0	495
	30(3)A		38.1	9.8	0.8	490
	30(3)B		38.5	9.0	0	489
	30(4)B		37.8	9.9	0	518
42-3, 140-150	peelings	391	38.6	20.0	11.9	474
	20(1)		36.7	10.1	1.3	455
	30(2)		34.4	9.6	0.8	465
45-4, 140-150	20(1)	421	33.4	10.3	1.2	459
	30(2)		32.0	10.3	0.6	412
48-3, 140-150	20(1)	448	27.2	10.7	2.7	394
	30(2)		25.6	10.7	1.2	

changes in Cl⁻ are real and, therefore, they need to be explained in terms of physical processes occurring in the accretionary prism.

Analytical Results

The results of the analytical program for the determination of major dissolved constituents of the interstitial waters obtained during ODP Leg 110 are presented in Table 2.

Because only relatively few samples were studied for the content of bromide, the results are reported separately as the Br⁻/Cl⁻ ratio in Table 3. Similarly data on the ⁸⁷Sr/⁸⁶Sr were deter-

mined on a few selected samples and these data are presented in Table 4.

LITHOLOGIES

The lithologies of the Leg 110 drill sites, together with those of DSDP Sites 541 and 542, are presented in Figure 3. The lithologic columns of Figure 3 follow the drill sites from the seaward side of the accretionary prism onto the prism (Fig. 1).

Several features are of importance in the following discussions:

1. The décollement zone was penetrated at Site 671, and was reached at Sites 541, 675, and 676. At Site 672 a zone of proto-décollement was penetrated between 180-210 mbsf.

2. Carbonate sediments predominate in the Pleistocene-Pliocene sections, as well as in the deeper Oligocene-Eocene sections of Sites 671 and 672.

3. The occurrences of volcanic ash are especially noticeable in the Pleistocene-Pliocene sections (Masclé, Moore, et al., 1988), as is seen in Figure 4 for Sites 671, 672, and 674.

4. In all sites arcward of the deformation front, increased folding, faulting, and overthrusting characterizes the sediment columns. As a result rapid thickening of the sediment column occurs.

PREVIOUS STUDIES—LEG 78A

Studies of the interstitial water composition of the three drill sites of DSDP Leg 78A (Gieskes et al., 1984) have revealed that alteration of volcanic material, dispersed in the sediments, plays an important role in causing increases in dissolved calcium and decreases in dissolved magnesium and potassium.

Site 543 was drilled north of the Leg 110 transect (Fig. 1) and reached Layer 2 basement at a relatively shallow depth of about 410 mbsf. The upper 200 m of the sediment column are characterized by the presence of ash beds and carbonates are restricted to the upper 75 m of sediments of Pleistocene-Pliocene age. Average sedimentation rates in the upper 200 m of the sediment column are about 20 m/m.y. Interstitial water concentration-depth profiles for Ca²⁺, Mg²⁺, Sr²⁺, ⁸⁷Sr/⁸⁶Sr of dissolved Sr²⁺, and δ¹⁸O (H₂O) are presented in Figure 5. The concentration-depth profile of Mg²⁺ indicates a minimum at about 150 mbsf and the rapid decrease in the upper 100 mbsf is accompanied by a rapid increase in Ca²⁺. Associated with this is a sharp decrease in ⁸⁷Sr/⁸⁶Sr, sharply below contemporaneous seawater values (DePaolo and Ingram, 1985; Hess et al., 1986; Palmer and Elderfield, 1985). Previous studies of interstitial water compositional change in sediments characterized by important contributions of volcanic material to the sediments have shown that the above observations can best be understood in terms of *in-situ* alteration reactions involving uptake of magnesium and ¹⁸O, release of calcium, and exchange of less radiogenic ⁸⁷Sr/⁸⁶Sr with the dissolved strontium in the interstitial waters (Gieskes and Lawrence, 1981; Gieskes et al., 1986, 1987). At depths below 300 mbsf the gradients in Ca²⁺ and δ¹⁸O (H₂O) and to a lesser extent the gradient in Mg²⁺ indicate that exchange with underlying basement rocks occurs (McDuff, 1981; Lawrence and Gieskes, 1981).

Sites 541 and 542 both failed to penetrate through the décollement, although both holes terminated in the close vicinity of this detachment surface. Drilling at Site 541 ended in the upper part of the décollement zone, and at Site 542 it ended in the frontal thrust that splays off the décollement at that location. Interstitial waters again indicate rapid increases in calcium and decreases in magnesium, especially in the upper sections, which are rich in volcanic ash (Figs. 6 and 7). Appreciable amounts of carbonates characterize the Quaternary and Pliocene sediments and, as a result of dissolution and/or recrystallization, substan-

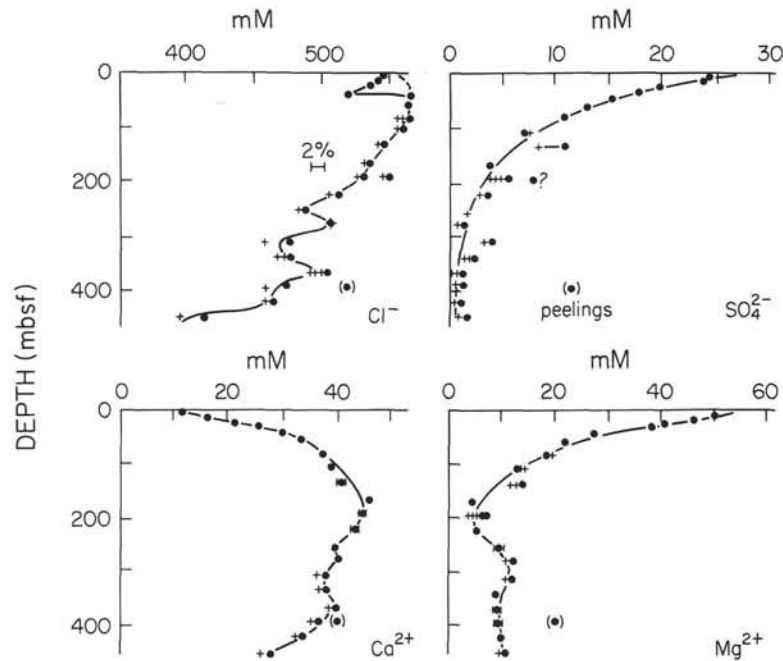


Figure 2. Results of sequential sampling for interstitial waters at Site 674. Dots: Initial squeeze at about 2000 psi. Crosses: Subsequent aliquots obtained at about 2000 and 3000 psi.

tial increases in dissolved strontium occur. Notwithstanding this, sharp decreases in the $^{87}\text{Sr}/^{86}\text{Sr}$ ratio of dissolved strontium occur, again suggesting the importance of alteration of volcanic matter in these sediments. Changes in dissolved calcium, magnesium, and $\delta^{18}\text{O}$ in the upper sediment column are larger at Sites 541 and 542 when compared with Site 543, mainly as a result of faster Quaternary sedimentation rates and an associated decrease in diffusive exchange with the overlying ocean.

LEG 110 SITES

In the following a brief description is presented of the interstitial water data obtained in the various drill sites occupied during ODP Leg 110. Of these, Sites 672, 671, and 674 are of special importance and therefore these sites are presented first, followed by Sites 673, 675, and 676, respectively.

Site 672

Site 672 was intended as the reference hole of the Leg 110 transect and for this purpose was located 6 km east of the toe of the accretionary prism. The lithologies and ages of the sediments are presented in Figure 3. Of importance are the radiolarian-rich sediments at the depth range of 180–210 mbsf. The lithology and age of this horizon is identical to the stratigraphic horizon along which the décollement develops at Site 671 (cf., Fig. 3). Structural features such as mud-filled veins and low-angle and high-angle shear zones with cm-scale displacements suggest the development of incipient deformation at this level. Furthermore, physical property measurements record high porosities here. These data suggest that the deformation is propagating along this horizon in front of the deformation front and that it marks the location of the “future décollement” (Moore, Mascle, et al., 1987). The oldest sediments drilled at this site are early Eocene in age and thus the site was terminated well above basement with an estimated age of about 140 Ma.

The concentrations of dissolved chloride (Fig. 8) show clear decreases with depth, minima centering at about 200 mbsf (zone

of “future décollement”) and in the sandstone layers at about 370 mbsf. Elsewhere (Blanc et al., 1988) we have reported slightly elevated methane concentrations at 200 mbsf and in the sandstones. These observations were interpreted in terms of advective flow of low chloride, methane-bearing solutions from deeper in the accretionary complex. A problem arose with a few selected samples, which showed chloride concentrations well above those of bottom water. These samples also showed elevated ammonia concentrations and precipitation of iron oxides upon storage. We are not willing to discard these data *a priori*, but we do not understand the reasons for the high Cl^- values. Are they the result of squeezing artifacts or the result of *in-situ* membrane filtration processes? Data for Ca^{2+} , Mg^{2+} , and SO_4^{2-} do not appear to be affected and follow normal trends.

An alkalinity (HCO_3^-) profile was obtained to a depth of 300 mbsf. Just below the interface at about 20 mbsf a small maximum occurs, followed by a well-established minimum of about 1.1 mM at about 120 mbsf. Lack of samples below 300 mbsf prevented a precise characterization of alkalinity changes at greater depths. The dissolved sulfate profile indicates a continued depletion in sulfate with depth to about 400 mbsf, thus indicating that the major source for the alkalinity increases is the production of HCO_3^- during the sulfate reduction process. The concentration depth profile of dissolved ammonium shows that the largest increases in NH_4^+ occur in the upper 60 m, probably as a result of organic matter alteration associated with bacterial sulfate reduction processes.

The concentration changes in dissolved calcium and magnesium are affected by several processes, which include the alteration of volcanic ash (as was also observed in the Leg 78A sites) in the upper 125 m. In addition, deep-seated reactions cause increases in Ca^{2+} and decreases in Mg^{2+} , perhaps as a result of alteration reactions involving underlying basement rocks (Gieskes, 1983; McDuff and Gieskes, 1976; McDuff, 1981). Unfortunately, basement was not reached at this site. Increases in Ca^{2+} far exceed the decreases in Mg^{2+} and typically a sharp decrease in Na^+/Cl^- is observed. Na^+ concentrations were obtained

Table 2. Interstitial water data: Major constituents, Sites 671-676.

Hole 671B

Core-Sec	Interval cm	Depth m	pH	Alkalinity mM	Salinity	Cl mM	SO ₄ mM	NH ₄ μM	Ca mM	Mg mM	Sr μM	Li μM	K mM	Na mM	Na/Cl	Si μM
1-3	145-150	4.5	7.89	3.09	35.0	559	27.6	35	11.9	50.6	102	28	12	492	0.88	530
2-5	145-150	16.0	7.69	4.10	35.0	564	27.8	55	12.8	49.9				498	0.88	480
3-4	145-150	22.0	7.68	2.67	35.5	570	25.0	115	16.0	45.1	169	30.5	12	500	0.88	212
4-5	145-150	33.0	7.70	2.13		574	22.8	160	18.0	42.3				501	0.87	228
6-4	145-150	50.5	7.74	1.56	34.7	570	20.8	180	20.7	39.6	213		9	492	0.86	220
8-4	145-150	68.5	7.76	1.41	34.4	568	18.0	210	23.5	34.6				489	0.86	184
10-3	145-150	86.0	7.89	0.85	34.2	571	16.6	220	25.2	32.9	233	22.5	6	488	0.85	240
13-3	145-150	113.0				559	14.8	240	28.0	30.8				471	0.84	240
14-6	84-89	125.0				570	13.0	270	30.2	27.0				481	0.85	510
15-1	59-65	127.0				572	13.6	540	28.1	24.4	280	27.8	9	495	0.87	520
17-4	145-150	153.0				573	13.2	520	27.3	27.1	301	28.3	7	490	0.86	640
19-1	145-150	171.0	7.62	1.05	34.0	569	12.8	390	26.2	26.9	320		6	488	0.86	250
22-5	145-150	200.0	7.69	0.92		570	13.2	325	27.6	26.1				489	0.86	250
25-4	145-150	230.0	7.74	1.02		570	14.6	260	28.6	26.5				489	0.86	228
28-5	145-150	260.0	7.72	0.71	34.2	564	15.0	240	30.7	24.8	518	23.2	5	482	0.86	275
31-1	145-150	290.0	7.38	0.64		560	16.2	230	30.8	25.0				480	0.86	230
33-2	16-22	310.0				554	16.2	320	33.0	22.9				474	0.86	200
34-3	140-150	320.0	7.54	0.70	32.3	533	15.6	215	36.0	22.9	483	28.9	4	446	0.84	230
37-2	140-150	348.0	7.43	1.85	33.0	539	18.0	195	36.1	24.3				455	0.84	240
40-3	140-150	368.0	7.65	1.05		539	16.6	185	39.1	22.6				449	0.83	252
41-4	93-101	380.0					16.6	265	39.5	20.4				451	0.84	180
43-3	140-150	397.0	8.11	1.02	32.7	536	19.1	210	37.1	25.4	232	38.9	4	450	0.84	170
46-3	140-150	420.0			32.4	526	15.0	215	40.2	22.7				431	0.82	175
49-3	140-150	450.0	7.86	1.70		523	19.0	195	40.7	25.5	190	72.5	3	430	0.82	300
52-2	140-150	477.0	7.63	2.24	32.5	520	17.0	235	40.3	27.0	192	69.5	3	421	0.81	260
55-5	140-150	508.0				505	13.9	225	37.2	28.1				404	0.8	815
56-2	139-150	516.0				508	14.0	260	36.3	30.9	182	146.6	4	403	0.79	650
58-6	140-150	535.0				552	13.0	240	39.9	37.1				426	0.77	250
61-5	140-150	566.0	7.73	2.78	37.2	556	11.2	315	43.6	38.8	271	214	4	415	0.75	220
63-5	140-150	580.0	7.52	2.47		560	9.5	320	46.0	38.0				413	0.74	280
65-5	140-150	600.0				547	8.6	330	49.6	39.3				388	0.71	240
67-5	140-150	620.0				564	7.8	355	55.7	37.6				394	0.7	230
70-5	140-150	650.0	7.23	2.80	34.3	563	6.6	355	64.9	36.6	352	316.2	3	375	0.67	275
73-5	140-150	675.0				508	6.0	340	66.1	33.6				322	0.63	440
74-1	16-22	685.0				542	8.7		72.4	34.0	240	45	4	348	0.64	375

Hole 672A

Core-Sec	Interval cm	Depth m	pH	Alkalinity mM	Salinity	Cl mM	SO ₄ mM	NH ₄ μM	Ca mM	Mg mM	Sr μM	Li μM	K mM	Na mM	Na/Cl	Si μM
1H-4	145-150	6.0				560	26.3	0	11.6	51.5	88	25	12	477	0.852	369
2H-6	145-150	12.0	7.43	2.99	35.5	563	27.1	27	12.7	49.9						420
3H-4	145-150	18.0	7.65	3.19	36.0	563	25.4	60	14.1	48.0	108	22	11	482	0.856	218
4H-5	145-150	29.0	7.68	3.20	35.3	562	26.6	30	13.7	48.2						337
5H-5	145-150	38.5	7.70	2.05	35.3	563	25.2	125	16.6	44.7	127	17	8	485	0.861	195
7H-5	145-150	57.5	7.81	1.74	35.0	563	24.2	206	19.3	41.9	150	21	9	482	0.856	169
9H-5	145-150	76.0	7.70	1.26		562	23.3	225	21.8	39.1						137
12H-5	145-150	105.0	7.79	1.17		562	22.5	232	26.2	36.7	187	21	6	477	0.849	168
15x-3	140-150	130.0	7.96	1.13	34.5	559	21.5	215	29.0	35.9	199	28	6	467	0.835	151
18X-3	140-150	158.0	7.90	1.85	34.3	552	21.1	230	32.2	38.4	212	55	5	449	0.813	150
21X-2	140-150	185.0	7.60	1.32	35.0	565	20.4	400	32.8	35.0	217	127	7	464	0.821	1030
24X-5	140-150	216.0	7.70	2.06	35.0	540	17.9	223	34.7	41.6		169				428
27X-5	140-150	245.0	7.69	3.33	34.2	554	16.8	210	37.4	42.2	291	231	5	427	0.771	255
30X-5	140-150	274.0	7.80	3.46	34.0	549	15.3	245	40.4	42.8						253
32X-4	140-150	290.0	7.70	4.47	35.0	549	14.1	255	42.2	41.8	310	330	4	411	0.749	323
34X-4	140-150	309.0	7.40	5.49	35.0	573	12.8	345	44.5	38.9	258	372	4	433	0.756	572
36X-4	140-150	327.0		5.17	34.2	532	13.9	235	50.2	42.1		377				463
38X-5	145-150	346.0			33.8	518	12.1	265	51.1	40.9		386				612
39x-2	145-150	352.0	7.69		36.2	576	13.0	560	53.2	38.2	329		6	419	0.727	740
40X-5	145-150	367.0			32.2	505	11.8	305	52.6	39.0						606
41X-1	145-150	376.0					10.8	280	52.7	35.9						509
42X-2	145-150	382.0			33.0	522	10.3	335	51.3	37.5	320		4	367	0.703	777
43X-4	145-150	395.0				529	12.4	320	56.5	37.5						682
46X-1	140-150	425.0			34.3	535	12.0	300	62.7	37.7						622
48X-3	140-150	447.0			34.0	527	15.8	315	61.6	38.8	325	339	3	361	0.685	472
51X-2	140-150	470.0				545	13.9	325	71.9	36.4						773
53X-4	145-150	489.0	6.52	7.64	33.8	572	11.8	405	79.2	35.4	340	391	4	370	0.647	676

Hole 673A

Core-Sec	Interval cm	Depth m	pH	Alkalinity mM	Salinity	Cl mM	SO ₄ mM	NH ₄ μM	Ca mM	Mg mM	Si μM
1-4	145-150	6	7.24	2.79	34.5	552	25.1	95	12.6	50.6	405
2-5	145-150	16	8.18	2.76	33.5	535	22.1	135	16.3	45.2	222
3-6	145-150	28	8.25	2.41	33.8	547	18.3	165	21.3	34.4	606
4-2	145-150	35	8.33	2.93	33.8	556	16.8	200	22.3	33.6	655

Table 2 (continued).

Hole 673B

Core-Sec.	Interval cm	Depth m	pH	Alkalinity mM	Salinity	Cl mM	SO4 mM	NH4 μM	Ca mM	Mg mM	Sr μM	Li μM	K mM	Na mM	Na/Cl	Si μM
1-4	145-150	6	7.79	2.88	34.70	549	25.3	60	13.0	50.1	56	52	10	466	0.85	529
2-5	145-150	15	8.08	2.65	34.50	559	23.1	130	16.5	43.1			9	481	0.86	345
3-5	145-150	24		2.46		569	19.6	205	20.4	36.9	107	32	8	488	0.86	458
4-5	145-150	34	7.79	1.37	34.00	563	17.0	235	23.2	31.7			8	480	0.85	317
5-4	145-150	42	8.20	2.18	33.50	559	14.8	250	26.7	28.6	152	30	6	474	0.85	148
7-1	145-150	57		1.49	33.00	555	11.2	360	30.0	21.6			5	470	0.85	120
9-3	145-150	79	7.96	1.74	32.20	551	5.1	470	34.0	14.5	164	119	5	460	0.83	730
12-2	140-150	105	8.10	3.01	32.00	549	5.2	530	32.0	15.9			5	461	0.84	
15-5	140-150	136	7.96	3.62	30.00	512	4.2	510	30.1	14.6	161	379	4	430	0.84	650
18-2	140-150	164			29.50	513	1.5	525	29.0	14.3			4	428	0.83	670
22-2	140-150	200			28.20	505	.0	525	29.2	13.5		316	4	418	0.83	185
25-4	140-150	230			31.00	541	3.6	600	31.1	15.8			4	453	0.84	177
28-5	140-150	260	7.73	2.97	32.20	543	.0	515	31.3	14.8	174	368	4	449	0.83	1103
31-6	140-150	290			28.20	491	.0	560	27.1	13.8	153		3	409	0.83	672
34-5	140-150	318	7.66	3.17	32.50	548	.5		31.4	15.7			3	454	0.83	

Hole 674A

Core-Sec.	Interval cm	Depth m	pH	Alkalinity mM	Salinity	Cl mM	SO4 mM	NH4 μM	Ca mM	Mg mM	Sr μM	Li μM	K mM	Na mM	Na/Cl	Si μM
1-3	145-150	4.5	7.86	3.51	34.2	546	24.3	8	11.5	50.1	84	97	10	465	0.85	420
2-6	145-150	15.5	8.15	3.34	34.0	543	24.0	82	15.8	46.4	104	40	9	461	0.85	180
3-5	145-150	23.5			33.5	537	20.0	145	21.2	40.8	127	104	6	450	0.84	175
4-3	145-150	30.0			32.0	518	18.0	155	25.2	38.4	143	57	6	423	0.82	455
5-4	145-150	40.5	7.73	1.32	34.3	569	15.5	235	29.8	27.5			5	481	0.85	400
7-2	145-150	57.0	6.87	.67	33.7	565	13.0	295	33.3	22.3	169	72	5	475	0.84	195
9-6	145-150	82.0				553	11.1	303	37.5	20.0	168	131	5	456	0.82	335
12-3	145-150	105.0	7.77	1.18	33.0	558	7.3	306	38.6	13.9	173	118	3	465	0.83	320
15-2	140-150	132.0	8.11	.93	33.0	543	8.5	243	40.6	12.5	170	31	2	453	0.83	210
18-2	140-150	165.0	8.07	1.20	31.8	530	4.0	287	46.2	4.9	187	37	1	436	0.82	200
21-3	140-150	190.0			32.2	527	4.8	433	44.5	5.1	177		2	437	0.83	225
24-5	140-150	220.0			29.0	501	2.4	313	42.7	5.0			2	410	0.82	130
27-5	140-150	250.0			26.5	481	1.6	317	38.8	9.5			2	388	0.81	930
30-3	140-150	275.0	7.85	2.88	29.5	508	.8	493	40.2	11.7			2	406	0.8	550
33-5	140-150	308.0			26.2	455	3.6	333	35.7	11.6	164	205	2	368	0.81	130
36-5	140-150	336.0				465	1.8	421	35.9	8.8		154	1	380	0.82	170
39-5	140-150	365.0				489	.0	380	37.8	9.9	160	214	1	395	0.81	935
42-3	140-150	391.0			25.5	455	.8	414	34.4	9.6	149	269	2	369	0.81	935
45-4	140-150	421.0				459	.4	398	32.0	10.3			1	377	0.82	120
48-3	140-150	448.0			23.5	394	1.0	322	25.6	10.7			1	324	0.82	285

Hole 675A

Core-Sec	Interval cm	Depth m	pH	Alkalinity mM	Salinity	Cl mM	SO4 mM	NH4 μM	Ca mM	Mg mM	
2-2	145-150	325				30	500	14	150	42.4	27.7
3-2	145-150	334				32.3	537	415.6	390	44.6	29.2
4-3	145-150	345				32	527	17.8	425	38.5	32.7
5-3	145-150	355	7.86	1.02		32	531	15.6	580	41.4	32.8
6-5	145-150	366				31.5	512	15.3	520	38.5	34.1
8-4	145-150	385				32.5	541	14.4	575	35.8	39.4

Hole 676A

Core-Sec.	Interval cm	Depth m	pH	Alkalinity mM	Salinity	Cl mM	SO4 mM	NH4 μM	Ca mM	Mg mM	Sr μM	Li μM	K mM	Na mM	Na/Cl	Si μM
1-3	145-150	5	7.88	4.71	34.2	558	25.5	25	12	49.8	98	25	11	479	0.858	
2-5	145-150	13	7.55	3.26	34	561	26	89	14.7	46.7	113	21	11	483	0.861	525
3-5	145-150	22	7.41	3.55	34.1	563	24	116	16	43.3	128	21	10	486	0.863	284
4-5	145-150	33	7.43	3	33.9	560	22.3	148	17.7	41.4	141	20	10	479	0.855	345
5-5	145-150	42			34	561	21.1	178	18.6	39.9	154	20	10	478	0.852	529
7-5	145-150	61	7.74	1.9	33.7	558	21.4	188	19.9	37.7			9	479	0.858	271
8-5	145-150	70	7.76	1.41	33.5	563	19.8	209	20.4	35.9	185	19	9	482	0.856	284
10-5	145-150	89	7.75	1.47	33.5	559	20.5	207	22.1	34.7			8	480	0.859	227
12-2	145-150	105	7.78	2.17	33.8	560	20.7	253	24.2	33.6	174	20	8	480	0.857	206
15-2	145-150	133	7.38	1.42	33.8	558	20.3	265	26.9	31.7			8	475	0.851	239
17-5	145-150	155	7.67	1.34	33.8	554	18.3	263	28.9	30.5	197		6	467	0.843	248
19-5	145-150	170	7.95	3.49	33.5	549	19	289	30	30.5			6	461	0.84	182
21-5	145-150	190	7.85	1.57	32.2	547	18	298	31	30.9	190	32	5	455	0.832	203
23-4	145-150	210			33.5	544	18.1	269	31.3	32.5			5	449	0.825	208
25-1	145-150	228			33.5	543	18.2	313	31	32.3	190	34	5	449	0.827	208
27-5	145-150	250			32	519	16.4	314	31.6	32.6			5	420	0.809	233
28-6	145-150	260			32.2	536	16.9	330	32.9	32.6	205	63	5	435	0.812	224
30-5	145-150	275	7.71	2.39	33.5	547	16.5	385	32.7	33.1			5	446	0.815	1225
31-3	145-150	286			32.5	537	18.3	340	29.5	36.4	195	123	5	438	0.816	1050
32-3	145-150	295			33	546	16	346	32.2	33.5			5	443	0.811	1220
33-5	145-150	305				548	15	378	30.9	36	226	56	5	440	0.803	1163

Table 3. Br⁻/Cl⁻ and NH₄⁺ in selected samples.

Hole	Core-section	Cl ⁻ (mM)	Br ⁻ /Cl ⁻	NH ₄ ⁺ (mM)
671B	4-5	574	0.00153	0.16
	22-5	570	0.00159	0.33
	34-3	533	0.00158	0.22
	55-5	505	0.00157	0.23
	56-2	508	0.00154	0.26
	74-1	542	0.00152	—
672A	3-4	563	0.00154	0.06
	18-3	552	0.00158	0.23
	21-2	565	0.00159	0.40
	34-4	573	0.00152	0.35
	38-5	518	0.00155	0.27
	39-2	576	0.00158	0.56
	43-4	529	0.00158	0.32
	674A	5-4	569	0.00158
15-2		545	0.00165	0.24
21-3		549	0.00159	0.43
24-5		503	0.00171	0.31
36-5		469	0.00175	0.42
45-4		459	0.00171	0.40
42-3		455	0.00171	0.41
48-3		394	0.00173	0.32

Table 4. Strontium isotope data, Leg 110.

Leg 110 Sample	⁸⁷ Sr/ ⁸⁶ Sr	±
671B-19-1	0.708267	24
671B-31-1	0.708490	32
671B-52-2	0.707245	26
671B-70-4	0.707504	30
672A-15-3	0.707708	30
672A-32-4	0.707755	24
672A-53-4	0.707380	36
674A-18-5	0.706599	34
676A-17-5	0.707735	28

from charge balance calculations. The Na⁺/Cl⁻ was used to suppress effects of decreasing chloride concentrations. The Na⁺/Cl⁻ profile, however, indicates that diffusive communication from greater depths has a strong influence on concentration profiles to a depth of about 100 mbsf. In the case of the Ca²⁺ profile, calcium concentration increases resulting from volcanic ash alteration reactions in the upper 170 m are superimposed on the gradient caused by reactions at greater depths. Because of the importance of Mg²⁺ uptake during volcanic ash alteration in the upper 170 m, however, a clear minimum in Mg²⁺ occurs at about 150 mbsf.

Strontium concentrations increase gradually with depth at this site, mainly as a result of carbonate recrystallization reactions.

The potassium concentration-depth profile (Fig. 8) indicates that a very rapid downhole decrease occurs in the upper 180 m. We interpret these observations in terms of potassium uptake in the clay formation process during volcanic ash alteration.

The lithium profile indicates that a source for this element exists in the early Oligocene and late Eocene sediments below 300 mbsf. Often increases in Li⁺ have been related to sediments rich in opaline silica (Gieskes, 1983), but at Site 672 the zone of future décollement at about 200 mbsf does not appear to constitute a source of dissolved Li⁺, notwithstanding elevated biogenic silica levels.

Dissolved silica concentrations are low above the zone of "future décollement", but within that zone a large increase oc-

curs (Fig. 8). Elevated silica concentrations below 300 mbsf are due to the presence of radiolarian silica.

Site 671

Site 671 is located at a distance of about 4 km arcward from the toe of the accretionary prism, slightly to the west of Site 541 (Fig. 1). The lithological and paleontological data, however, reveal a complex lithostratigraphy. This is particularly evident from repetition of the Pleistocene-late Miocene sediment section below about 128 mbsf as a result of major thrusting (Fig. 3). As a consequence of thrusting, the well-defined, relatively radiolarian-rich décollement zone, which was located at Site 672 at about 200 mbsf, now occurs at about 500 mbsf at Site 671, thus indicating a considerable tectonic thickening of the sediment column at only a short distance from the toe of the prism. The sediments below the décollement zone are tectonically relatively undisturbed, but we were not able to penetrate through the sand layers at the bottom of the site (Moore, Mascle, et al., 1987).

Dissolved chloride concentrations (Fig. 9) indicate a minimum in the décollement zone, as well as lower values just at the interface with the sands at the bottom of the hole. Above the décollement, irregularities in the Cl⁻ gradient indicate local inputs of low-Cl⁻ fluids along fault zones (Blanc et al., 1988). Again relatively high methane concentrations (though considerably less than 1 mM in concentration) are associated with these decreases in dissolved chloride (Blanc et al., 1988). We postulate later that these low-Cl⁻ concentrations and elevated methane concentrations are related to advection of waters along the décollement or through the sandstones from an origin much further to the west beneath the accretionary complex.

Similar to observations at Site 672, alkalinities show a shallow maximum, below which values drop rapidly to <1 mM, with an observed increase below the décollement. The concentration-depth profile of dissolved sulfate, however, is distinctly different from that of Site 672. A distinct minimum in dissolved sulfate occurs at about 150 mbsf, i.e., just below the top of the structurally repeated Pleistocene-Pliocene section. As a result of this process it appears that relatively more reactive organic carbon was buried below the 128 m of overburden, thus enhancing sulfate reduction. This is also demonstrated by a sharp maximum in ammonium.

In the upper 128 m, gradual increases in Ca²⁺ and decreases in Mg²⁺ with increasing depth are observed, but below 128 mbsf a reversal in these gradients is evident. The upper 300 m of the sediment column is characterized by the presence of volcanic ash (Fig. 4), and thus this is the zone where *in-situ* alteration of volcanic material can affect the Ca²⁺ and Mg²⁺ profiles (Gieskes and Lawrence, 1981). The shapes of the Ca²⁺ and Mg²⁺ profiles are complex, mainly as a result of the recent duplication of the upper sediment section by tectonic activity. Below the décollement a maximum in Mg²⁺ is observed similar to that found at Site 672. Also a very sharp increase in dissolved calcium occurs below the décollement, probably as a result of diffusive supply of Ca²⁺ from greater depths. As at Site 672, a large decrease in Na⁺ accompanies the increase in Ca²⁺. The Na⁺/Cl⁻ ratio shows a gradient below about 300 mbsf with a sharp decrease below the décollement zone (Fig. 9). It is of importance to note that while the diffusion of Na⁺ is recognized above the décollement over a distance of about 200 mbsf, the influence of the diffusive supply of Ca²⁺ from the deeper sections is not noticed above the décollement. This is probably due both to the slower diffusion of Ca²⁺ as well as to the maintenance of a relatively constant Ca²⁺ concentration by advective flow in the décollement zone. This problem is discussed in greater detail in a later section.

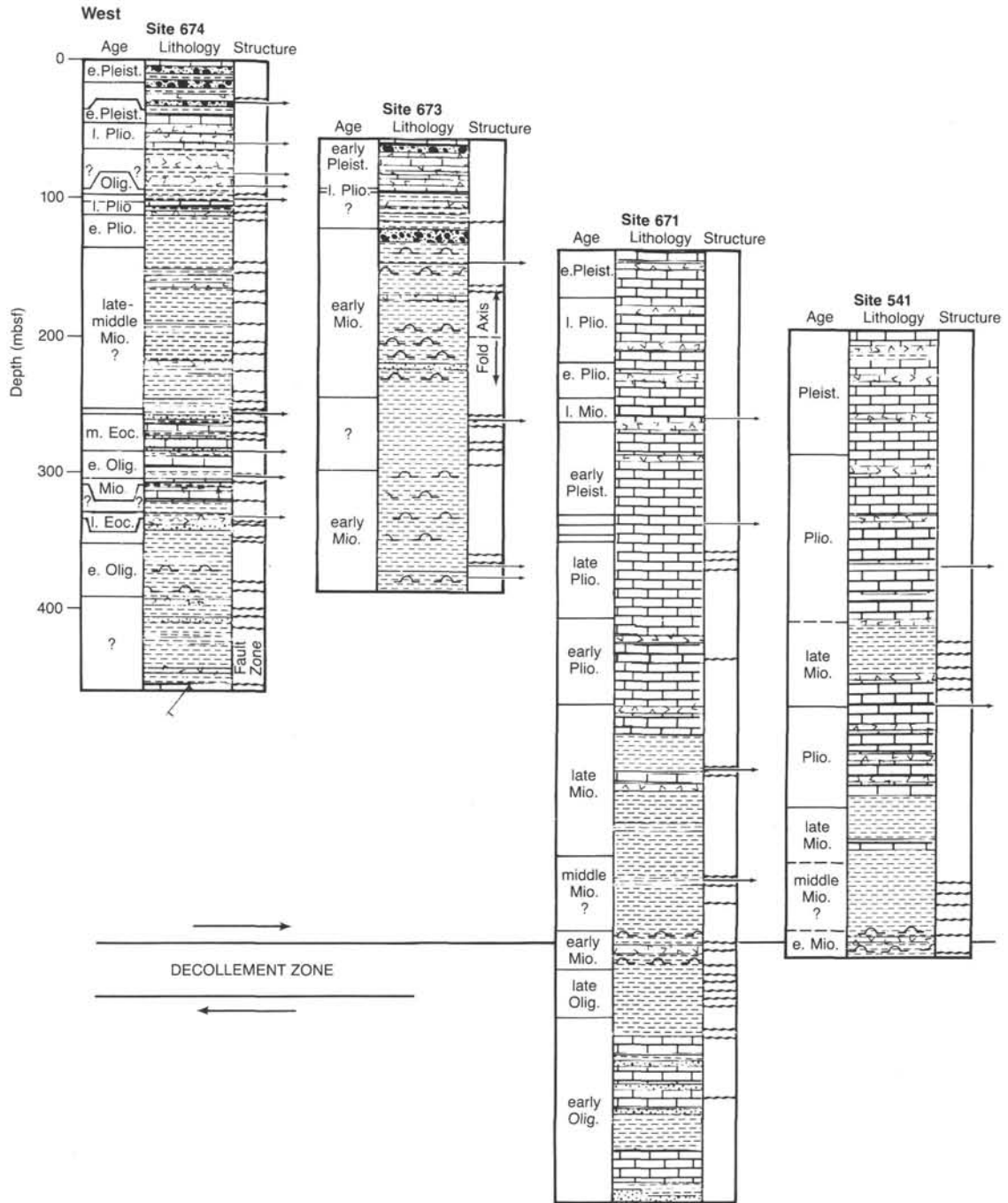


Figure 3. Lithologic summary columns of Sites along the Leg 78A and 110 drill-hole transect.

The sediment section between 400 mbsf and the décollement zone is essentially void of carbonate, but the overlying section has two maxima (Wang et al., this volume), a result of the repeated sediment sequence. The data of dissolved Sr^{2+} reflect this situation by a complex distribution of dissolved Sr^{2+} with depth. A pronounced maximum occurs at about 275 mbsf and is clearly related to carbonate recrystallization processes (Gies-

kes et al., 1986). Increases in Sr^{2+} below the décollement reflect the presence of calcium carbonate in the deeper horizons.

Depletion of potassium is strong in the upper volcanic ash-rich sediments and little change is observed below about 400 mbsf. This depletion is consistent with that observed at Site 672.

Concentration changes in lithium are very small in the upper 400 m, below which a gradual increase occurs leading to a maxi-

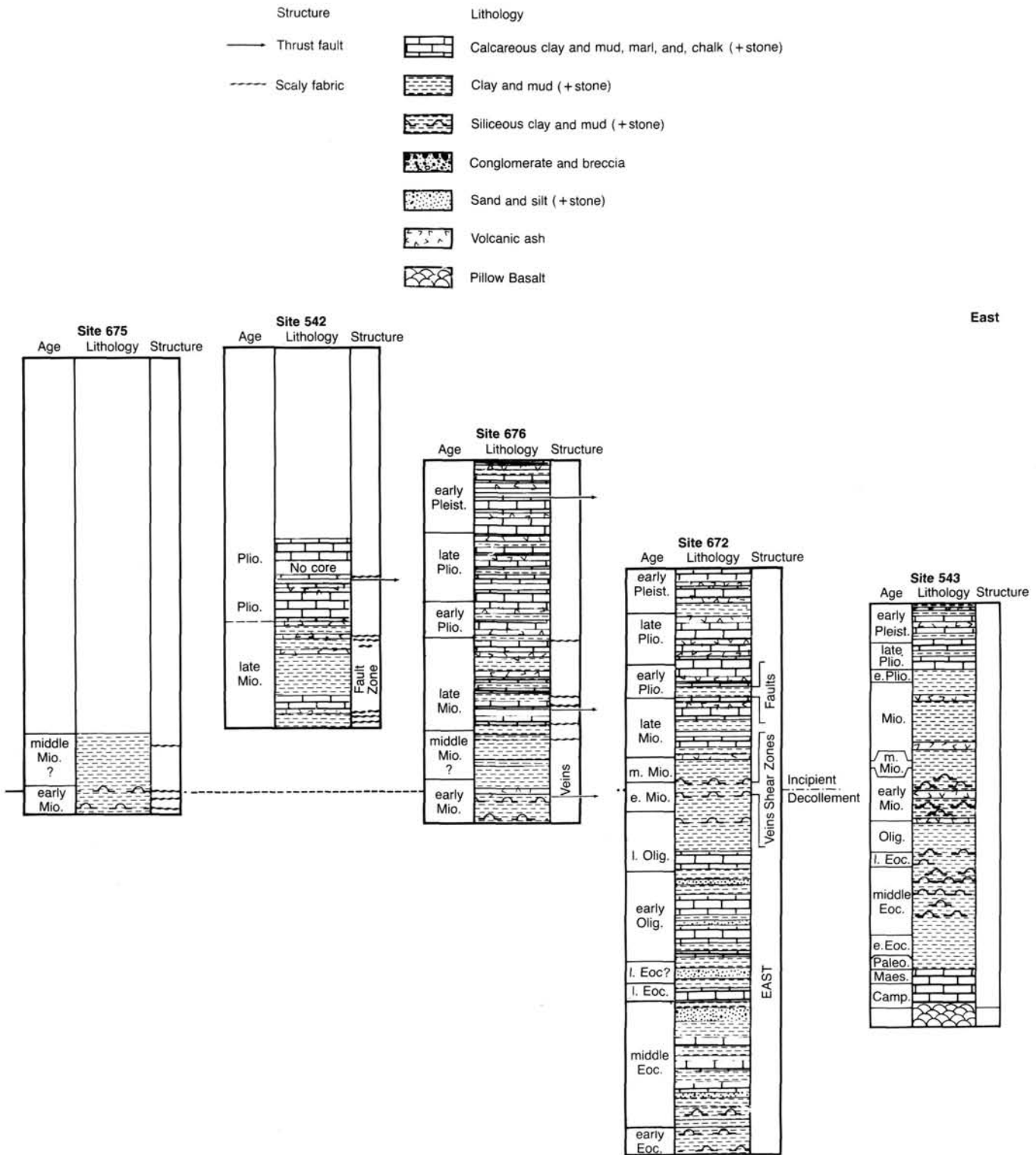


Figure 3 (continued).

imum in Li^+ at about 650 mbsf. Again, as at Site 672, the décollement zone, though somewhat enriched in siliceous material, does not appear to act as a source for lithium.

Dissolved silica concentrations are elevated in the Pleistocene sections, probably as a result of higher plagioclase and biogenic silica contents (Masclé, Moore, et al., 1988). Similar to Site 672 the décollement shows high dissolved silica concentration, as do

the lowermost sediments, which are slightly enriched in biogenic silica.

Site 674

The sediments at this site show a complex deformation pattern (Masclé, Moore et al., 1988), much more so than sites closer to the deformation front (e.g., Sites 541 and 671). Struc-

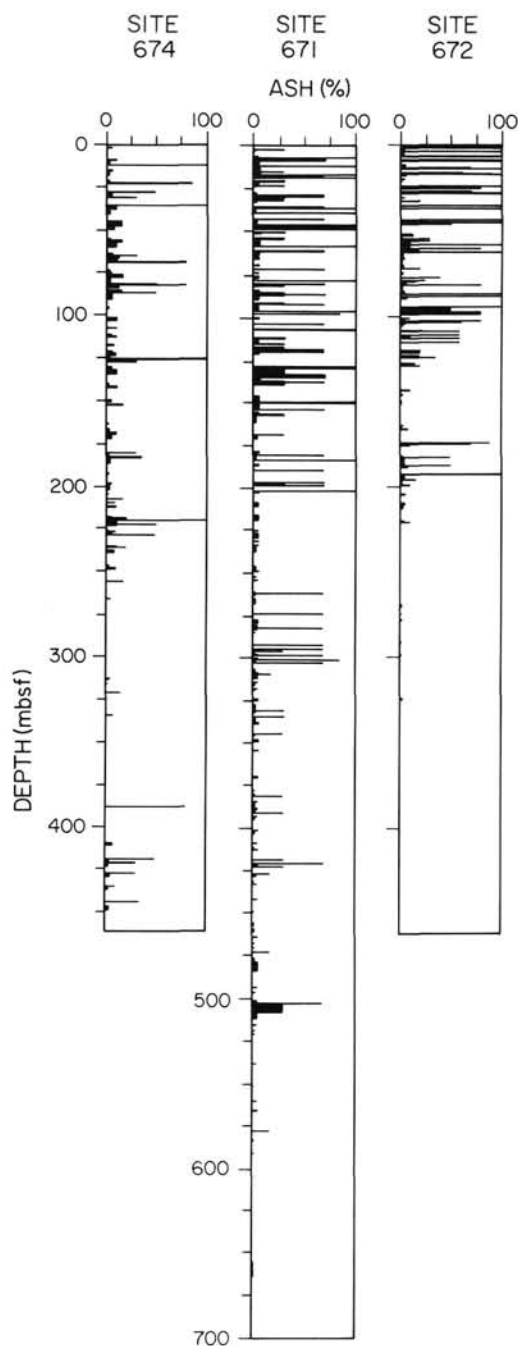


Figure 4. Distribution of ash layers in sediments from Sites 671, 672, and 674.

turally these sediments include overturned sections, scaly fabrics, stratal disruption, veining, and cataclastic shear zones, much as is observed in subaerially exposed accretionary complexes. Porosity studies show that notwithstanding the large amount of deformation, only a modest amount of dewatering has occurred, with porosities remaining above 50%. Major later thrust faults have been observed in these sediments, correlating well with landward-dipping seismic reflectors.

Chloride concentrations show a general decrease with depth in these sediments, with periodic minima associated with the above-mentioned later thrust faults (Fig 10). This is particularly evident at about 20 mbsf just below a Miocene(?) block of sedi-

ments. At this depth a sharp chloride minimum is associated with a well-defined positive temperature anomaly (Moore, Masle, et al., 1987; Fisher and Hounslow, this volume). The chloride minima at greater depths are also associated with fault zones (Moore, Masle, et al., 1987).

Few samples have been analyzed for alkalinity, but low concentrations are pervasive throughout the site, notwithstanding the large decrease in dissolved sulfate. Ammonia concentrations increase rapidly in the upper 50 m, i.e., in the zone of the highest decreases in dissolved sulfate.

Calcium and magnesium concentration depth profiles in the upper 30 m show a somewhat different curvature from the profiles of Sites 671 and 672. In part this may be due to the anomalous nature of the pore fluid, as is best exemplified by the chloride profile. Calcium concentrations reach a maximum at about 200 mbsf. We postulate that at greater depths removal of Ca^{2+} may occur as a result of precipitation of authigenic calcium carbonate. Magnesium concentrations show a minimum at about 200 mbsf and reach constant values below the silica-rich claystone layers at about 250 mbsf. This claystone layer is reminiscent of the sediments associated with the décollement at Sites 671 and 672.

Dissolved strontium concentrations increase gradually with depth to reach maximum values of about 180 M. Toward the bottom of the hole, however, decreases are observed. Carbonates are relatively unimportant in these sediments, but nevertheless recrystallization of this material is probably responsible for the observed increases.

Downhole decreases in potassium are very large in the upper 125 m of the sediment section, to reach the lowest concentrations observed during Leg 110.

Lithium concentrations remain low in the upper 200 m, below which distinct increases occur. The scatter in the upper 100 m is interpreted in terms of analytical problems, rather than as real variability.

Dissolved silica concentrations reflect the presence of biogenic silica in these sediments with typical maxima at 250 mbsf and 380–400 mbsf.

Site 673

This site is about 13 km from the deformation front and consists of two major lithologic units. Unit 1 from the seafloor to about 74 mbsf consists of Pleistocene and Pliocene calcareous muds and marls with minor contents of ash, and is interpreted as a slope deposit. Unit 2 consists of hemipelagic middle and lower Miocene claystones and siliceous claystones. Considerable faulting and overturned folding mark these sediments.

Chloride concentrations show complexity throughout the section drilled (Fig. 11). Hole 673A shows a near surface minimum, which appears absent in Hole 673B. At greater depths low Cl^- occurs mainly at thrust faults. The variability in the profile suggests that low-chloride fluids were periodically injected into these sediments at recent enough times for diffusive smoothing to have been ineffective.

Alkalinities remain low throughout the sediment column (Table 2), but sulfate shows a strong decrease with depth to become essentially zero below 200 mbsf. Ammonia concentrations show a steady increase to about 110 mbsf, and then remain constant below this depth.

Concentration gradients in dissolved calcium and magnesium occur in the upper 80 m of the sediment column, i.e., throughout Unit 1. This implies that below about 80 mbsf no significant reactions occur that involve a net transport of Ca^{2+} or Mg^{2+} to or from the solid phases.

Dissolved strontium reaches a constant concentration below Unit 1, and remains at about 160 μM .

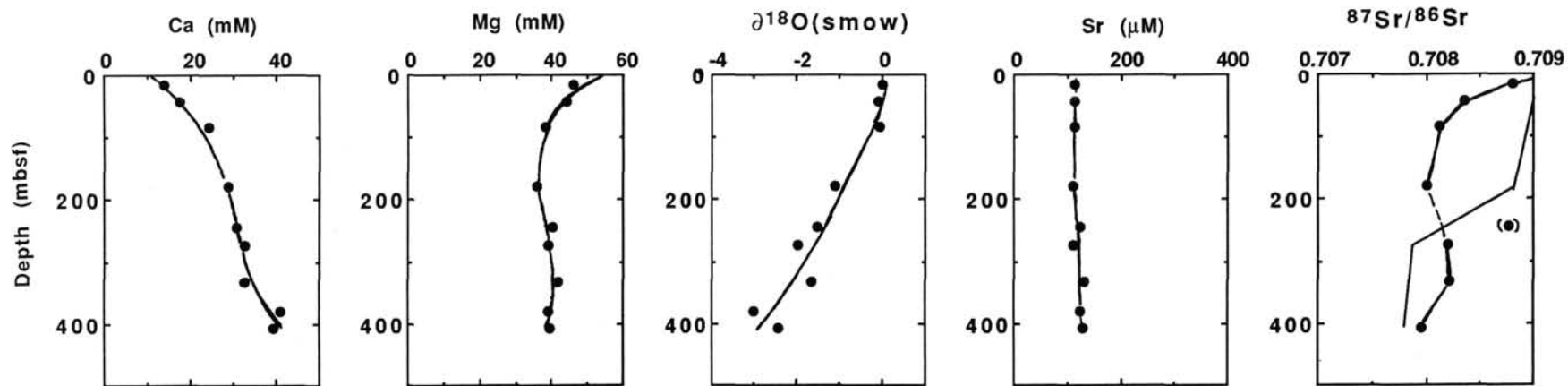


Figure 5. Interstitial water chemistry, DSDP Site 543. The solid line is for $^{87}\text{Sr}/^{86}\text{Sr}$ of contemporaneous seawater, and the datum in parentheses is questionable.

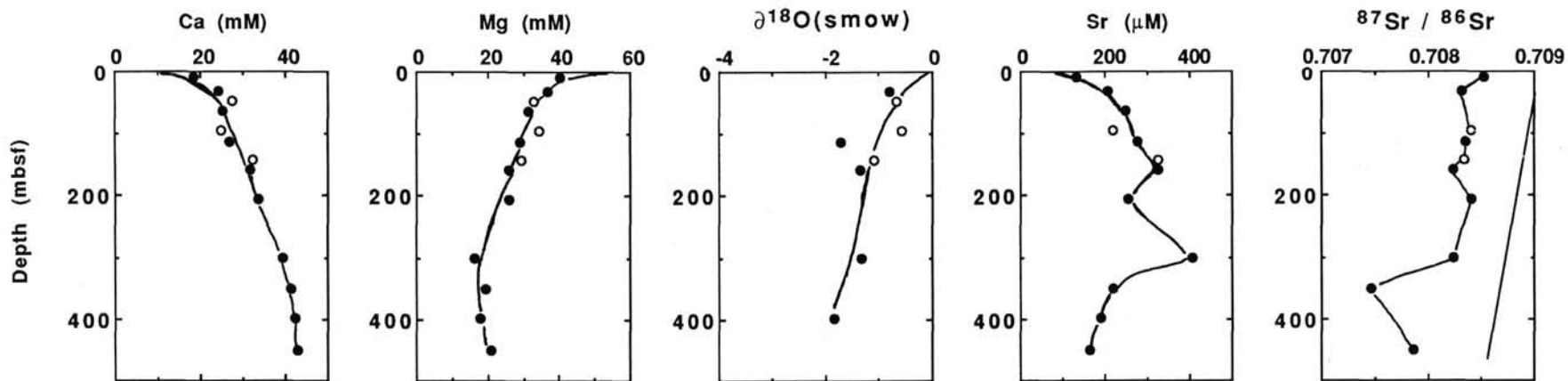


Figure 6. Interstitial water chemistry, DSDP Site 541. Open circles represent *in-situ* samples. Dashed line is for $^{87}\text{Sr}/^{86}\text{Sr}$ of contemporaneous seawater.

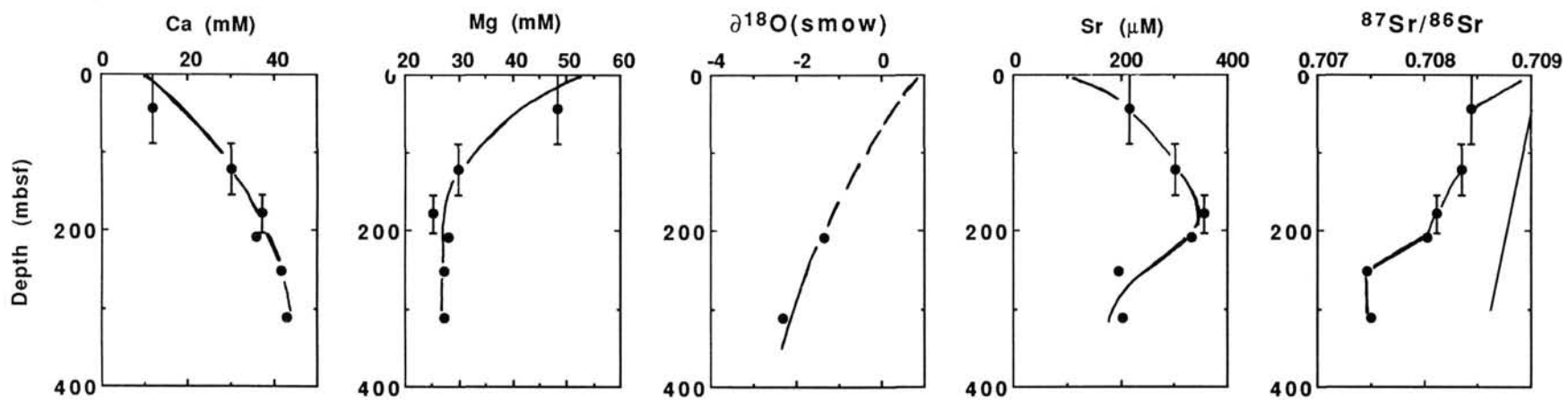


Figure 7. Interstitial water chemistry, DSDP Site 542. Vertical bars represent uncertainties of depth of wash-core samples. Dashed line is for $^{87}\text{Sr}/^{86}\text{Sr}$ of contemporaneous seawater.

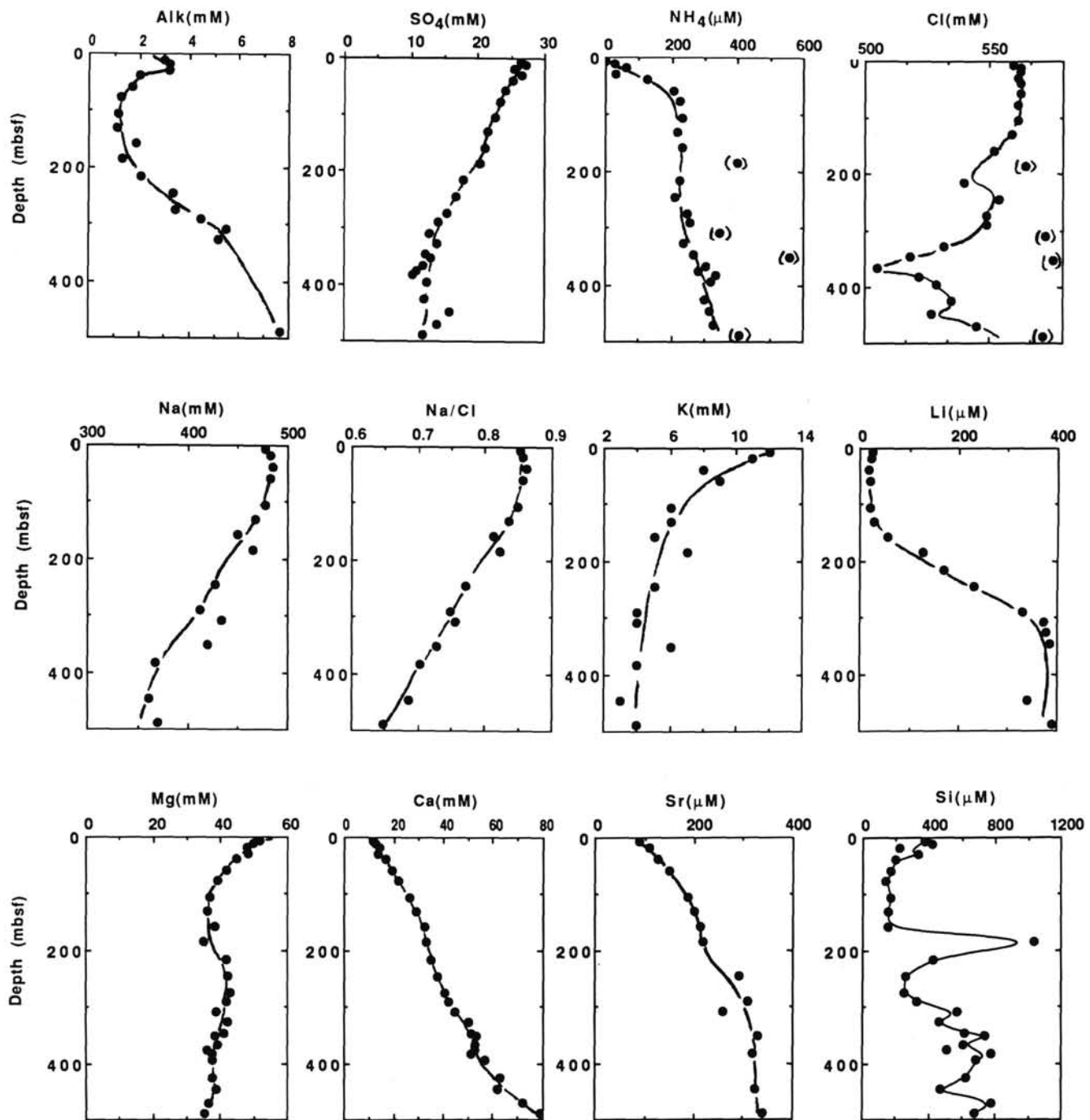


Figure 8. Interstitial water chemistry, Site 672. Data in brackets represent samples high in Cl^- ; c.f. text.

The Na/Cl ratio remains essentially constant throughout the sediment column, indicating no significant removal of Na^+ , which only covaries with the Cl^- concentration.

Dissolved potassium rapidly decreases in the upper 80 m (Unit 1), below which almost constant concentrations are reached. Lithium concentrations, on the other hand, increase rapidly in Unit 2.

Silica concentrations are highly variable and represent variations in biogenic silica.

Site 675

Site 675 was drilled near DSDP Site 542 of Leg 78A. The principal purpose of this hole was to carry out a packer experi-

ment and to sample the zone of décollement for lithology and geochemistry. Unfortunately, as with its predecessor, hole conditions forced abandonment of the site. Notwithstanding the slight difference in site locations (Fig. 1), we have combined the profiles of Sites 542 and 675 to suggest the possible geochemistry in Hole 675 in the uncored section above 325 mbsf.

The chloride concentrations (Fig. 12) show strong variability with depth, suggesting the presence of fault zones above the actual décollement, much the same as at Site 671. Hole conditions were unfavorable, especially near Cores 110-675A-6X and -7X, probably related to zones of potential movement of low-salinity waters. The data strongly suggest that coring started in or very near a major fault zone.

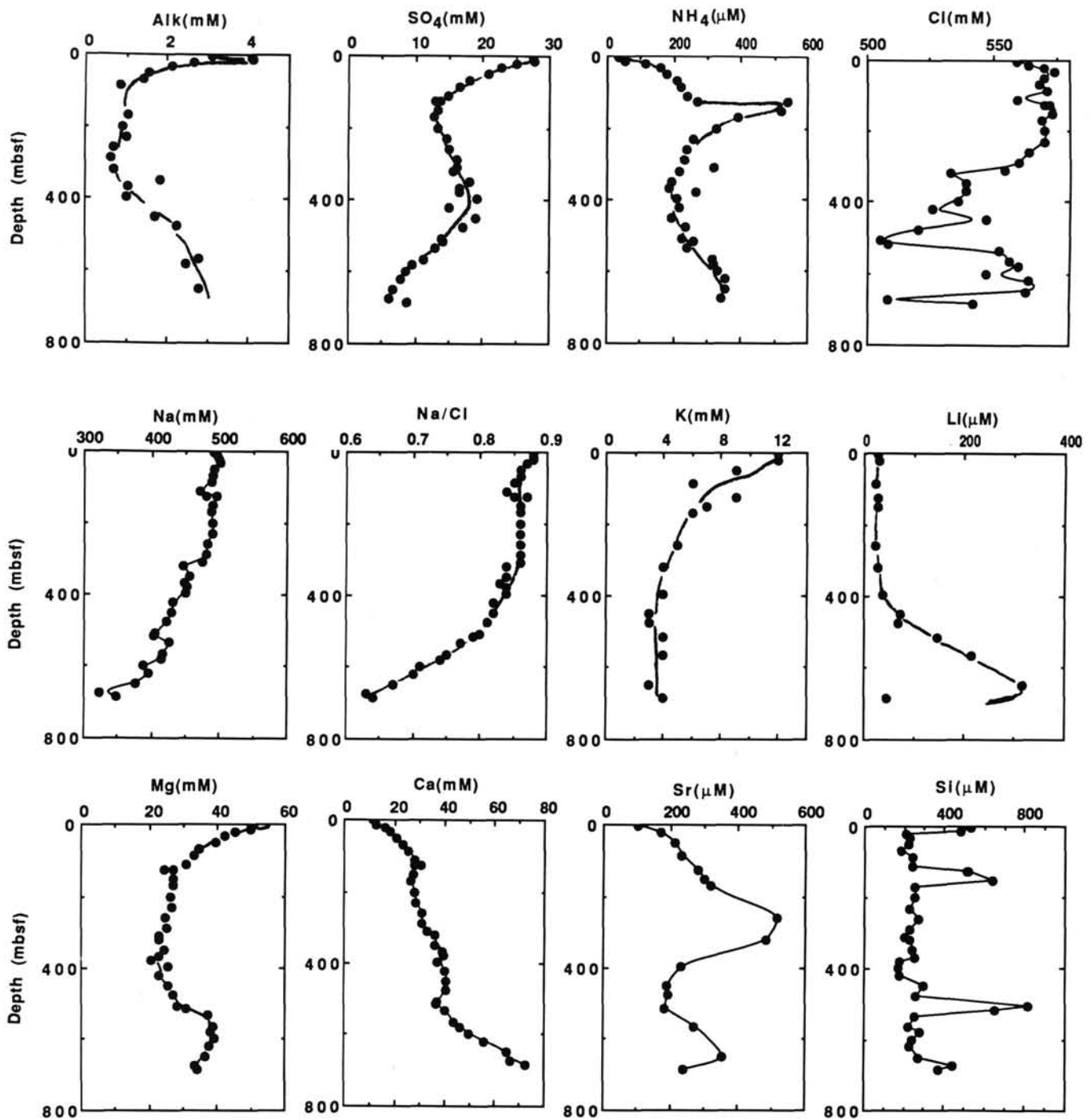


Figure 9. Interstitial water chemistry, Site 671.

The data on sulfate and ammonia for Hole 542 are not of sufficient quality for an adequate comparison. However, dissolved SO_4^{2-} is lower at Site 675 (Table 2) than in the décollement zone of Site 671, and similarly NH_4^+ concentrations are much higher. This may well be related to the higher rates of sedimentation in the upper part of the hole; typically Site 542 has a much higher sedimentation rate than Site 671. These differences are probably related to structural complications in both holes.

The concentrations of calcium and magnesium in Hole 675A suggest that indeed Hole 542 can, as a first approximation, be considered as a precursor of Hole 675A. This is so, notwith-

standing the along-structural-strike distance of about 1200 m between the sites. The data suggest that in this area a certain lateral homogeneity exists in Ca^{2+} and Mg^{2+} profiles above the décollement zone. Perhaps the termination of Hole 542 was caused by a cave-in associated with a fault above the décollement similar to the situation here. The Ca^{2+} and Mg^{2+} profiles show distinct gradients toward the décollement, with the magnesium gradient being quite similar to that observed directly above the décollement of Site 671.

Concentrations of dissolved silica are particularly high in Cores 110-675A-6X and -8X, i.e., in the zones rich in radiolari-

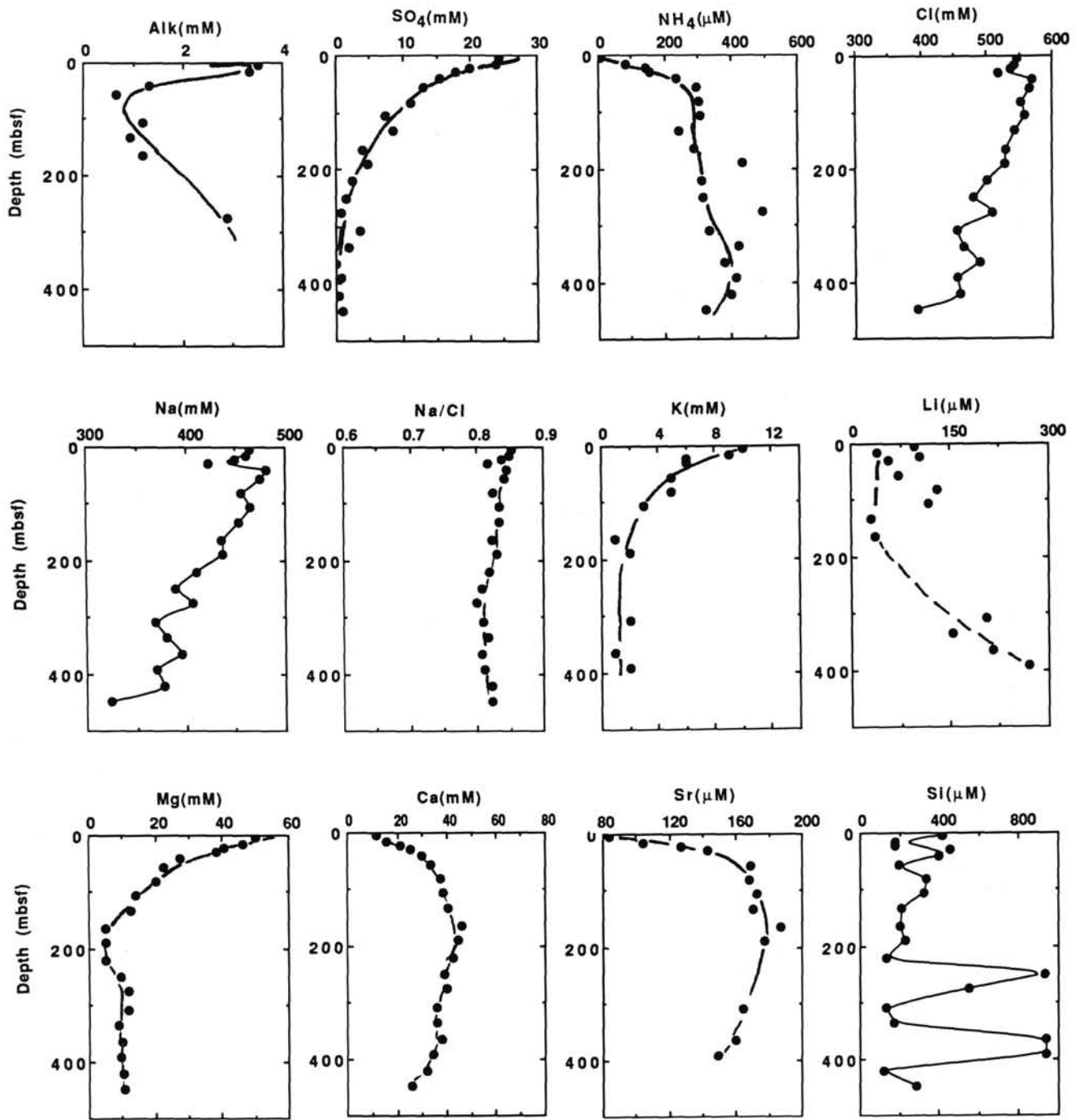


Figure 10. Interstitial water chemistry, Site 674. Scatter in Li^+ data in upper 100 m is probably due to error.

ans. Silica in Core 110-675A-8X is typical for the yellowish sediments associated with the décollement of Sites 671 and 672 (future décollement). Higher values of silica also occur in barren Core 110-675A-2X and this may be related to the potential occurrence of a nearby fault.

Site 676

This site is located only 250 m arcward of the deformation front and was drilled to investigate the incipient stages of accretion. The décollement zone occurs below 270 mbsf at this site, typically represented by large enrichments in dissolved silica (Fig. 13).

The profile of dissolved chloride indicates the occurrence of a minimum at about 250 mbsf. A steady decrease with depth in the Cl^- concentration to the zone of the Cl^- minimum suggests that the observed minimum is real. Unfortunately, the core just above the minimum was recovered empty, so that the curvature drawn in Figure 13 is somewhat tentative.

Alkalinities remain relatively low, notwithstanding the relatively large depletions in dissolved sulfate. The dissolved sulfate profile suggests a relatively large depletion in the upper 60 m, i.e., in the more rapidly accumulated sediment section. Similarly, the dissolved ammonia concentrations also increase rapidly over the same depth interval.

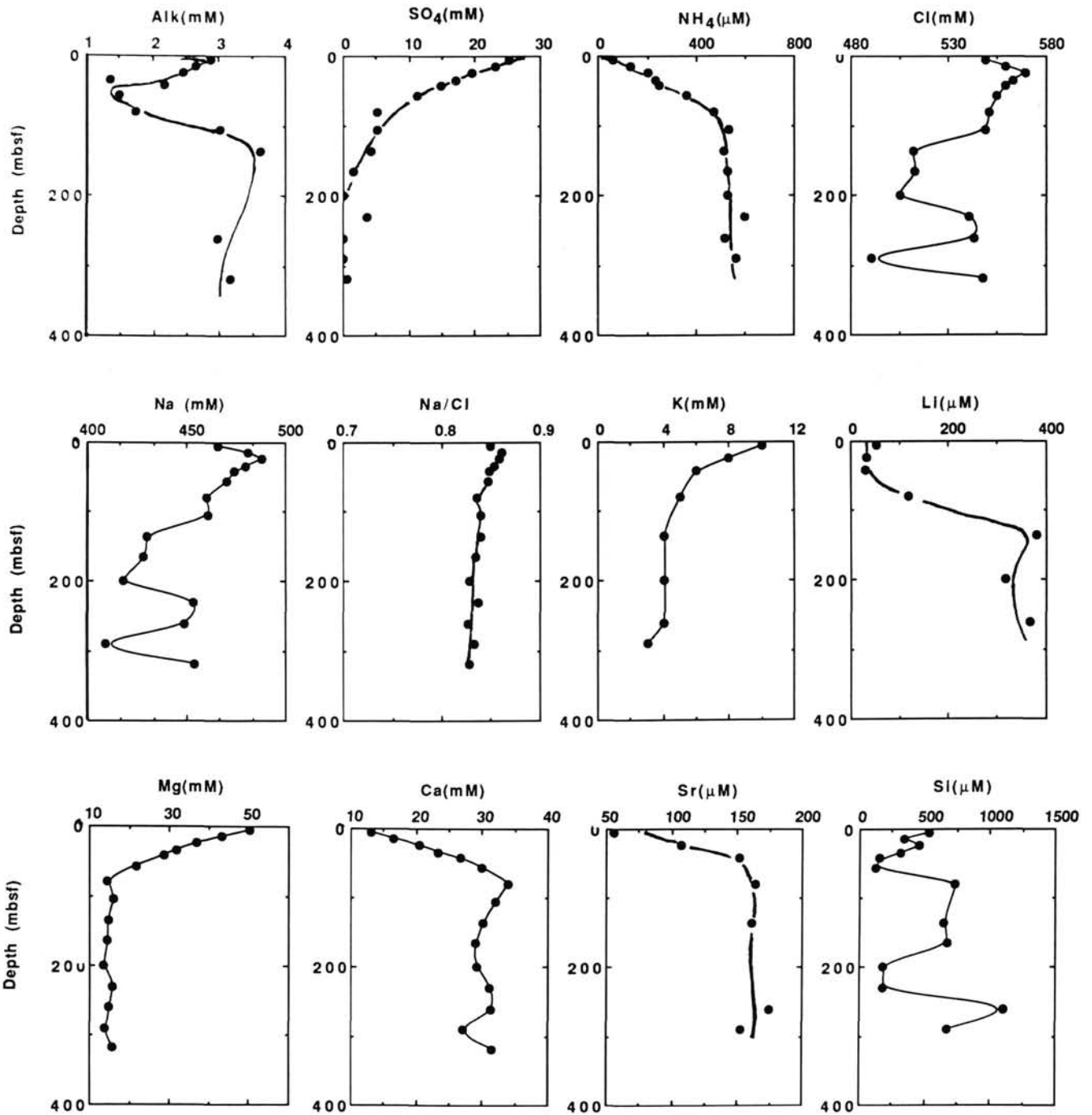


Figure 11. Interstitial water chemistry, Site 673.

Downhole increases in dissolved calcium and decreases in dissolved magnesium are largest in the Pleistocene–Pliocene volcanic ash-rich sediments. Below 200 mbsf a reversal occurs in the Mg^{2+} profile, similar to that in profiles in Sites 671 and 672 just above the zone of décollement.

Increases in dissolved strontium are relatively modest, but they do occur in the carbonate-rich sediments of the upper 150 m of the sediment column, presumably as a result of calcium carbonate recrystallization.

A sharp decrease occurs in dissolved potassium in the upper 200 m, below which concentrations remain constant. Lithium concentrations have a source at about 300 mbsf or below this depth. Sodium concentrations largely reflect those of chloride,

but as expected from a comparison with profiles from Sites 671 and 672, a progressive decrease can be observed toward the zone of décollement.

CHLORIDE ANOMALIES

As noted before, all of the drill sites of Leg 110, and to some extent also Sites 541 and 542 of Leg 78A (Gieskes et al., 1984), show well-defined decreases in chloride associated with the zone of décollement, the sandstone layers below the décollement, or recent fault zones in the upslope Sites 673 and 674. A generalized diagram of these decreases for Sites 671, 672, and 674 is presented in Figure 14.

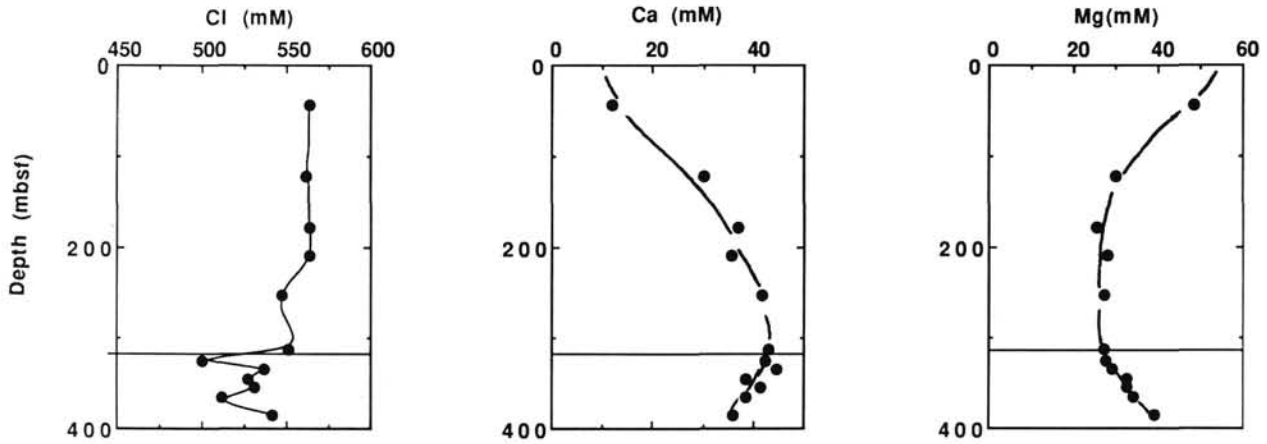


Figure 12. Interstitial water chemistry, Site 675. Data above 320 mbsf are for Site 542 (c.f., Fig. 7).

Decreased chloride concentrations have been noticed previously at DSDP sites in various settings. Low-chloride concentrations at Site 241 of DSDP Leg 25 (Gieskes, 1974) and at Site 438 of DSDP Leg 57 (Moore and Gieskes, 1980) were attributed to the influence of meteoric waters flowing through aquifers or trapped as a result of subsidence. At these sites there was no evidence for the occurrence of gas hydrates, even though organic gases were present at Site 438. In other areas, however, especially in drill sites across the Middle American Trench (e.g., Harrison et al., 1982; Hesse et al., 1985; Gieskes et al., 1985), low chloride concentrations have been explained in terms of dilution artifacts caused by the decomposition of gas hydrates during the pore-water retrieval process. Similar observations have been made on the Blake Bahamas Plateau during DSDP Leg 76 (Jenden and Gieskes, 1983). Hydrate decomposition leads to increases in $\delta^{18}\text{O}(\text{H}_2\text{O})$ as a result of melting.

Any artifacts caused by hydrates can be ruled out for Leg 110 sediments because methane gas concentrations, even in the décollement zone (Blanc et al., 1988), never exceed millimolar concentrations. For these reasons low chlorides cannot be explained in terms of hydrate decomposition *in situ*. Hydrates are commonly observed in the much more rapidly accumulated accretionary sediments to the south of the transect, and we cannot rule out that deep decomposition of such hydrates has led to the advection of low-chloride fluids toward the décollement zone of the Leg 110 transect. Another possibility is that the lower chloride concentrations are caused by dilution effects as a result of freshwater production by dewatering of clays. Indeed, there is evidence from clay mineralogical studies that burial diagenesis of clays already occurs in the sediments below the décollement of Site 671 (Jane Schoonmaker Tribble, pers. comm.). Such dewatering may be even more likely under the higher temperature and pressure conditions caused by the tectonic thickening of the sediment column further up the complex. In addition such dewatering processes may be accompanied by membrane filtration processes, which would lead to expulsion of low-chloride fluids characterized by low $\delta^{18}\text{O}(\text{H}_2\text{O})$ values and low Br^-/Cl^- ratios (Coplen and Hanshaw, 1973; Hanshaw and Coplen, 1973; Marine and Fritz, 1981). That freshwater production does occur further in the complex appears to be supported by the chloride decreases along three types of conduit: (a) faults in the accretionary complex; (b) the zone of décollement; and (c) through sandstones in the underthrust sequences (Moore, Mascle, Taylor, 1987; Beck, et al., 1988). The major question, however, is as to the location in the accretionary complex, where the postulated dewatering processes occur and whether membrane filtration processes are contributors to the chemistry of the fluids.

Vrolijk et al. (this volume) discuss the evidence for the various dewatering processes in the light of the information on the oxygen and hydrogen isotopic compositions of the fluids. These authors suggest that membrane filtration processes are relatively unimportant at these sites because of increases or decreases in $\delta^{18}\text{O}$ and δD of the pore waters, and that the processes leading to low chloride concentrations in the accretionary complex also seem to lead to overall increases in $\delta^{18}\text{O}(\text{H}_2\text{O})$. Despite the lack of good correlation between low chloride concentrations and increases or decreases in $\delta^{18}\text{O}$ and δD , their interpretation of the overall trend of increased $\delta^{18}\text{O}$ would rule out the importance of membrane filtration processes, since this latter mechanism would tend to reduce $\delta^{18}\text{O}$ along with Cl^- .

In the following we discuss measured Br^-/Cl^- ratios as well as the occurrence of shallow Cl^- anomalies associated with heat-flow anomalies at Site 674 with the specific purpose of further investigating the processes that led to the observed depletions in chloride.

Bromide-Chloride Ratios

In this study we have carried out a series of analyses of the ratio of Br^-/Cl^- in samples from Holes 671B, 672A, and 674A. The data are presented in Table 3 and Figure 15.

Whereas in Holes 671B and 672A there are no significant changes from the present-day seawater Br^-/Cl^- ratio (0.00155), the data for Site 674A indicate a small increase of perhaps as much as 10%. This increase may be due to the production of bromide during the diagenesis of organic matter. Recent studies in our laboratory as well as elsewhere (M. von Breyman and E. Suess, pers. comm.) have shown consistent increases in Br^-/Cl^- in deep-sea drill core interstitial waters from organic carbon-rich sediments. Thus, if anything, the decrease in chloride concentration is accompanied by a small increase in the Br^-/Cl^- ratio. If membrane filtration is the cause of the decrease in chloride, a simultaneous decrease in Br^-/Cl^- should occur (Kharaka and Berry, 1973). We conclude that the Br^-/Cl^- ratio cannot be used directly as an indicator of membrane filtration. At the same time, if hydrate decomposition led to the observed chloride decreases, a much larger signal in Br^-/Cl^- would be expected (Wang and Gieskes, 1988).

Chloride Minima at Sites 673 and 674

Prominent features of the chloride concentration depth profiles in Holes 673A and 674A are the clearly established minima at very shallow depths (Fig. 16). These minima occur in sediments of anomalous (Miocene?) age, i.e., in sediments that appear to have been replaced by tectonic activity between sedi-

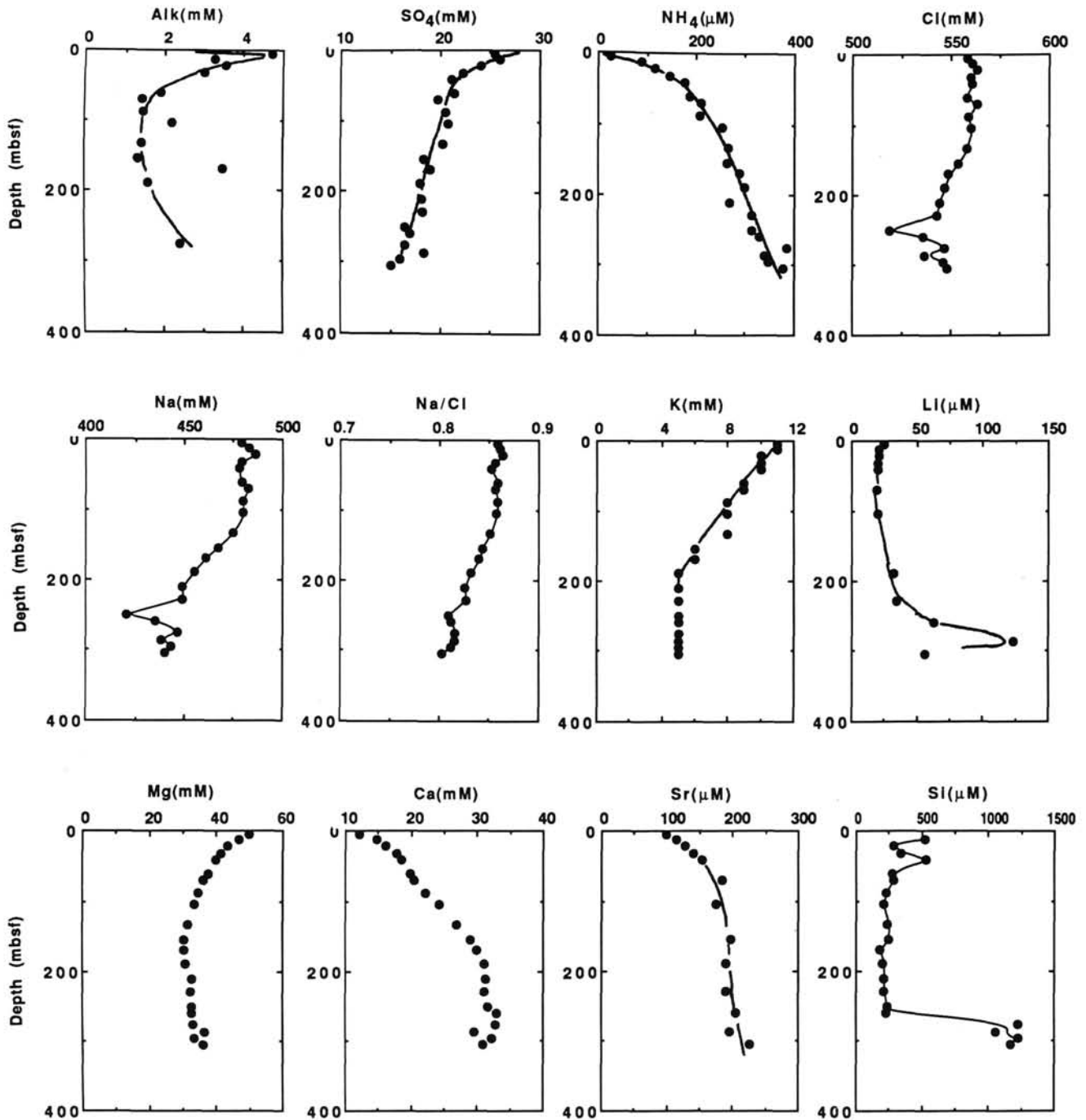


Figure 13. Interstitial water chemistry, Site 676.

ments of much younger age. Associated with these low-chloride concentrations are temperature anomalies of considerable magnitude. At Site 676 no chloride anomaly was observed, but here also a clear temperature anomaly occurs at shallow depth. It has been suggested that the above anomalies can be understood in terms of advective flow of warmer waters along fault zones (Fisher and Hounslow, this volume). In this section we attempt to evaluate this suggestion in terms of the observed concentration-depth profiles of interstitial water constituents.

Whereas the chloride anomaly in Hole 674A is quite evident in the upper 50 m, the concentration-depth profiles of calcium, magnesium, and sulfate do not allow one to distinguish anoma-

lies. For these reasons we have plotted the concentrations of calcium and sulfate as a function of magnesium in Figure 17 for the entire data sets of Holes 673B and 674A, and a similar plot for the upper part of Hole 674A is given in Figure 18 (including chloride concentrations). Though the choice of magnesium as a reference is arbitrary, any anomalies in the other constituents may show up in these correlation plots. From Figure 18 it is evident that reasonably linear relationships between the constituents characterize the upper part of the sediment column (also compare with Figs. 10 and 11). However, the data in the zone of minimum chloride in the upper part of Hole 674A show small, but distinguishable, differences from this linearity for sulfate

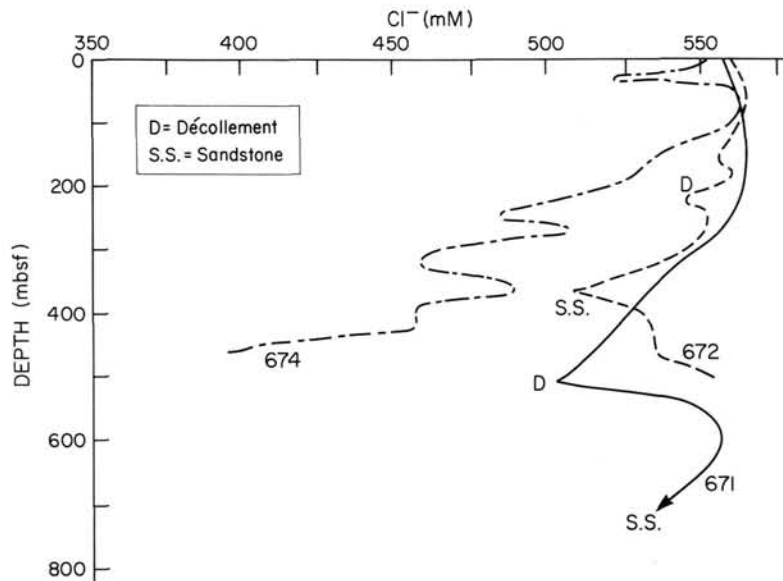


Figure 14. Generalized composite of Cl^- profiles of Sites 672, 671, and 674. Note progressive Cl^- decrease onto the accretionary prism (from 672 to 674).

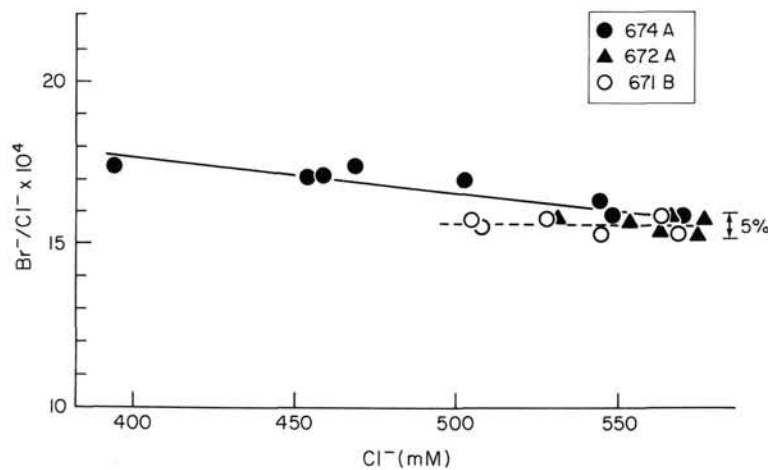


Figure 15. Br^-/Cl^- data of interstitial waters at Sites 671, 672, and 674 as a function of Cl^- concentration.

and calcium (Fig. 18). The largest anomaly in SO_4^{2-} is about -2 mM, and in Ca^{2+} about $+3$ mM, i.e., the anomalies are of relatively small magnitude.

If the chloride minima are an inherited property of the older sediment block that has been emplaced at shallow depth in Hole 674A, then, assuming that concentration-depth profiles at Sites 673 and 674 are representative for this area, these Miocene(?) sediments must have originated from at least 120 mbsf at Site 673 and from about 200 mbsf at Site 674. This, taking Site 674 as an example, would imply that the pore fluids are characterized by very low magnesium and sulfate concentrations, and also by calcium anomalies larger than observed in Figure 18. Indeed, much-reduced values of $\delta^{18}\text{O}(\text{H}_2\text{O})$ values would be expected, whereas the observed values are relatively high. If advection of low-chloride fluids had occurred along the fault zone associated with the emplaced Miocene(?) block of sediments and if no large modification had occurred in the fluid composition, then again larger anomalies should have been observed. If, on

the other hand, advecting fluids along the thrust fault were to alter their composition as a result of exchange with the pore fluids from the surrounding sediments through diffusive or mixing processes, it is difficult to understand why only a clear signal would occur in the chloride concentrations, with only small signals in sulfate, magnesium, and calcium.

An alternative explanation would have to invoke the production of freshwater *in situ* or at relatively shallow levels nearby (presumably more arcward) as a result of an as yet unidentified physicochemical process, e.g., clay mineral dehydration or membrane filtration. Perhaps the former process has been enhanced as a result of the energy release associated with the processes leading to the thrust faulting. This process would lead to a dilution effect, thus explaining the relatively small changes in the other major constituents ($<10\%$) and also the slightly enhanced values of $\delta^{18}\text{O}(\text{H}_2\text{O})$.

None of the above discussions has offered a satisfactory solution as to the processes that lead to the observed large deple-

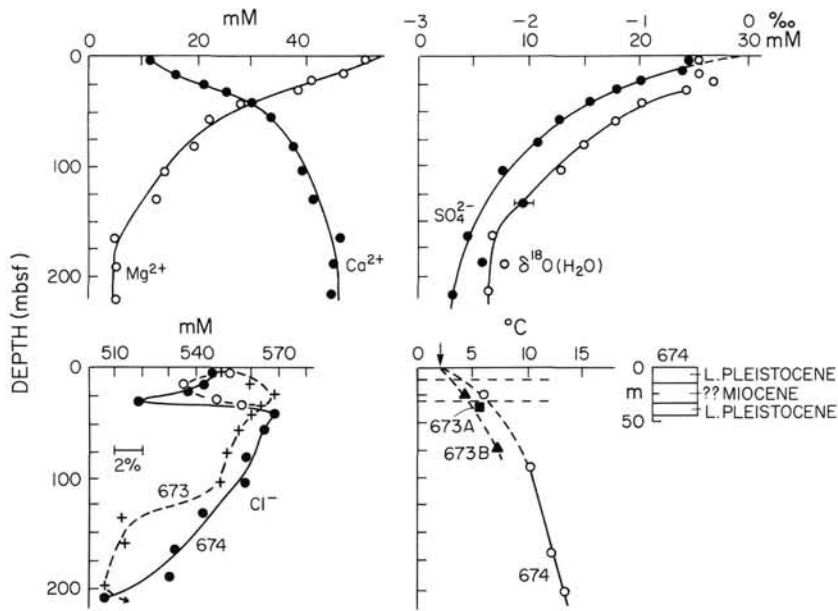


Figure 16. Details of concentration depth profiles in upper parts of Sites 673 and 674. Temperature data are from Fisher and Hounslow (this volume).

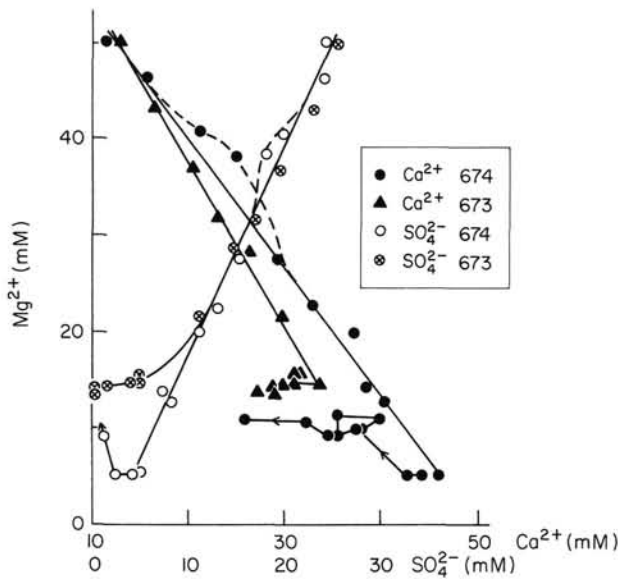


Figure 17. Correlation between Mg^{2+} , Ca^{2+} , and SO_4^{2-} for Sites 673 and 674.

tions in chloride concentrations. We postulate that clay mineral dehydration is a major contributing factor, but we cannot rule out other contributing factors, such as water flow from more southerly areas, which may be influenced by hydrate decomposition reactions. Also, potential effects of membrane filtration cannot be ruled out entirely, leaving an interesting question concerning the accumulation of brines farther in the deeper sections of the accretionary prism.

REACTIONS INVOLVING VOLCANIC ASH ALTERATION

At all sites drilled along the Leg 110 transect it is apparent that significant uptake of magnesium and potassium and release

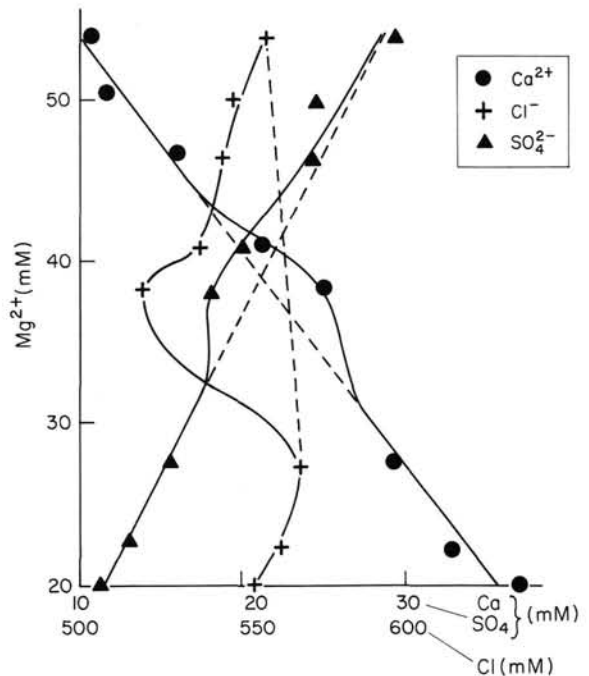


Figure 18. Correlation between Mg^{2+} and Ca^{2+} , SO_4^{2-} , and Cl^- for upper part Hole 674A.

of calcium occurs in the younger, volcanic ash-enriched sections. Indeed, a common observation is a minimum in Mg^{2+} above the zone of décollement. This phenomenon is well demonstrated in Figure 19, which presents a composite of magnesium profiles of relevant sites drilled along the Leg 78A/110 transect. Several phenomena are involved in establishing the Mg^{2+} concentration-depth profiles. Whereas the minima observed in Sites 672, 676, and 671 (and perhaps 541) profiles are related to processes involving the alteration of volcanic ash (as is

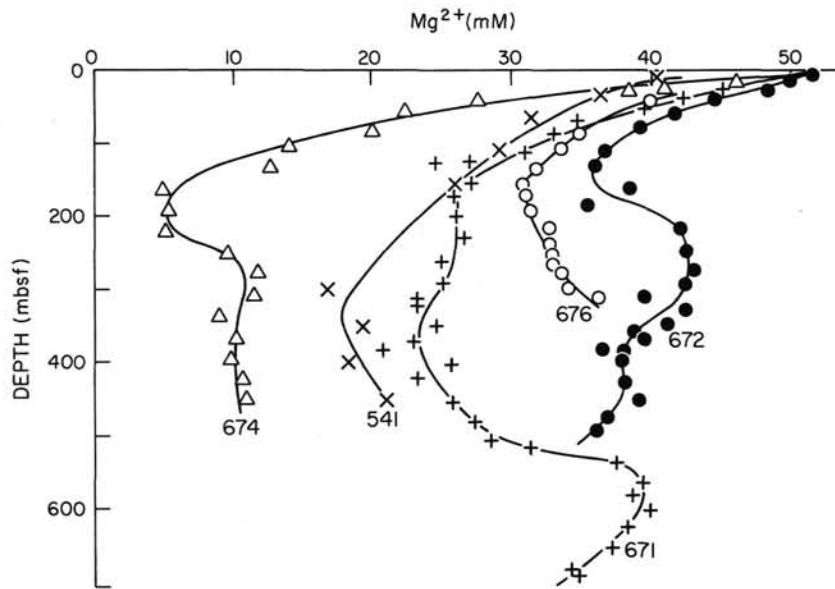


Figure 19. Composite of Mg^{2+} concentration-depth profiles of Sites 541, 671, 672, 674, and 676.

discussed in the section on $^{87}Sr/^{86}Sr$, various other processes may also have an influence on the shape of the profiles. Foremost among these are potential differences in sedimentation rates. At higher sedimentation rates the gradients in Mg^{2+} will increase because of a lessening resupply due to diffusion from the overlying ocean. Typically, sedimentation rates in the upper 100 m of Sites 672, 676, 671, and 541 have been 18, 21, 28, and 50 m per 106 yr. In addition, tectonic thickening of the sediments can also lead to increased depletions of Mg^{2+} . This can be the case for Site 671 where volcanic ash-rich sediments are buried to greater depths as a result of underthrusting. At Site 674 Miocene(?) sediments are intermixed with much younger sediments as a result of tectonic activity. This tectonic process has moved sediments depleted in Mg^{2+} up-section, but more importantly it interferes with the resupply of Mg^{2+} from the overlying ocean.

To understand the various profiles of Ca^{2+} and Mg^{2+} it is worthwhile to consider a correlation diagram between concentrations of calcium and magnesium (Fig. 20), using data for Sites 671, 672, 675 (+542), 676, and 541. Several features are apparent from this diagram. In the younger, volcanic ash-rich sediments, the data follow an almost linear relation, with lower Mg^{2+} and higher Ca^{2+} concentrations for sites with higher sedimentation rates (e.g., Site 541). Toward the décollement zone large changes in Mg^{2+} and distinct minima in Ca^{2+} occur particularly at Sites 671 and, presumably, 675, possibly associated with advecting low Cl^- waters along this zone. Below the décollement the data of Sites 671 and 672 coalesce into one linear relationship, with a slope of $\Delta Ca/\Delta Mg = -5$. Though basement was not reached at these sites we suggest that the deeper Ca^{2+} and Mg^{2+} concentration-depth profiles are the result of exchange with underlying basement (McDuff, 1981; Gieskes, 1983). The increases in Ca^{2+} are to some extent balanced by decreases in Mg^{2+} , but more so by decreases in Na^+ . If the data are extrapolated to zero Mg^{2+} concentrations, it follows that also the Na^+ concentrations in underlying basement will be very close to zero, the basement formation fluids constituting an almost pure $CaCl_2$ brine.

The minima in dissolved Mg^{2+} are accompanied by decreases in alkalinity, a phenomenon observed previously in sediments

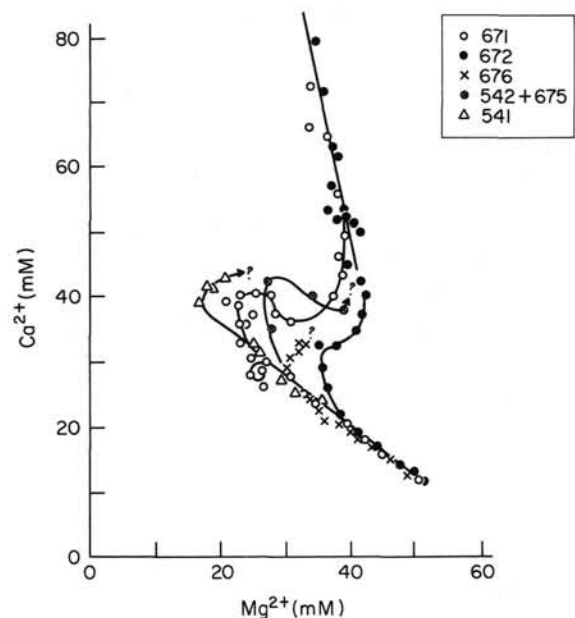


Figure 20. Correlation between Ca^{2+} and Mg^{2+} for Sites 541, 542+675, 671, 672, and 676.

that are affected by the *in-situ* alteration of volcanic ash in the sediment column (Gieskes et al., 1987). Thus the process of volcanic ash alteration leads to the uptake of magnesium and potassium (see site descriptions), a release of calcium, and a consumption of alkalinity (HCO_3^-), perhaps in part as a result of calcium carbonate precipitation. Changes in $\delta^{18}O$ (H_2O) of the pore fluids (Vrolijk et al., this volume) as a result of ash alteration are relatively minor compared to those occurring at greater depth. At this stage it is difficult to offer a quantitative assessment of the amount of *in-situ* alteration of volcanic ash. There is little doubt, however, that this process has a profound effect on the interstitial water chemistry.

Strontium Isotope Changes

Preliminary results of $^{87}\text{Sr}/^{86}\text{Sr}$ ratios of dissolved strontium are presented in Table 3 and in Figure 21. The latter figure includes information on Sites 541 and 543 of Leg 78A (Gieskes et al., 1984). It is clear that in the volcanic ash-rich sediments, strongly decreased $^{87}\text{Sr}/^{86}\text{Sr}$ ratios occur compared with the contemporaneous seawater curve. If increased Sr^{2+} concentrations were due chiefly to release from carbonates, the contributions of ash alteration reactions would be even larger than is apparent from the $^{87}\text{Sr}/^{86}\text{Sr}$ ratios. Unfortunately, deviations of strontium isotope ratios from contemporaneous seawater values cannot be used to obtain a quantitative estimate of the importance of volcanic ash alteration. For this purpose oxygen isotope mass-balance considerations are still the most appropriate, even though such calculations are not straightforward (Lawrence and Gieskes, 1981).

SUMMARY AND CONCLUSIONS

Studies of the major-element chemical composition of interstitial waters of sediments recovered in a transect of drill sites obtained during DSDP Leg 78A and ODP Leg 110 have revealed the importance of several processes in shaping the concentration-depth profiles of these constituents. Several important features have been identified:

1. Low-chloride fluids characterize the interstitial waters from the various sites drilled on the Northern Barbados accretionary complex (Fig. 22). We have established that low-chloride fluids are associated with methane anomalies in the décollement zone and in the underlying sandstones (Blanc et al., 1988). In the sites farther onto the accretionary complex, low-chloride fluids are not associated with methane anomalies. The origin of low-chloride concentrations can be best explained in terms of clay dewatering reactions, although other mechanisms such as gas hydrate decomposition reactions farther to the south in the complex or membrane filtration processes cannot be ruled out. Some of the chloride anomalies may well have been caused locally during the faulting process, although water migration cannot

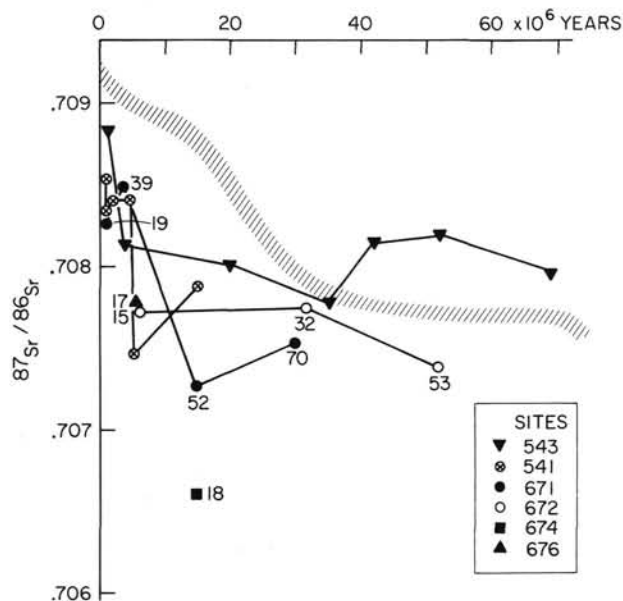


Figure 21. $^{87}\text{Sr}/^{86}\text{Sr}$ of dissolved Sr^{2+} of Sites 541, 543, 671, 672, 674, and 676. Shaded zone represents contemporaneous seawater range.

not be excluded entirely. Thus the geochemical evidence does support the idea of fluid migration along the décollement and fault zones during the dewatering of the accretionary complex.

2. Major cation concentration changes are affected by several processes in the sediments of the Leg 110 transect: (a) The upper Pleistocene-Pliocene sediments show evidence of magnesium and potassium uptake with some release of calcium as a result of volcanic ash alteration. The latter process has a strong influence on the $^{87}\text{Sr}/^{86}\text{Sr}$ ratio of dissolved strontium, but changes in $\delta^{18}\text{O}$ are mainly directed by diffusive processes from greater depths; (b) Complex tectonic processes, including folding and thrusting, have led to increasing depletions of magnesium, potassium, and sulfate as a result of decreased replenishment of these ions from the overlying ocean. This phenomenon is best demonstrated at Site 671, in which non-steady state profiles of Ca^{2+} , Mg^{2+} , and SO_4^{2-} characterize the interstitial fluid chemistry; (c) Below the décollement zone large increases in calcium and decreases in magnesium, sodium, and $\delta^{18}\text{O}$ (H_2O) indicate that exchange with deeply buried basement rocks may influence the interstitial water chemistry. Because the sites were terminated well short of basement, this argument remains speculative.

ACKNOWLEDGMENTS

We thank the shipboard chemistry technicians Katie Sigler and Matt Mefferd for their cheerful cooperation in the shipboard geochemical program. This research was, in part, supported by NSF grant OCE86-13517 (J.M.G.), as well as by the National Environmental Research Council of Britain (H. E.) and the Conseil National de Recherche Scientifique (G. B.). The paper was reviewed by R. E. McDuff and J. R. Lawrence.

REFERENCES

- Barnes, R. O., 1988. ODP in situ fluid sampling and measurement: a new wireline tool. In Mascle, A., Moore, J. C., et al., *Proc. ODP, Init. Repts.*, 110: College Station, TX (Ocean Drilling Program), 55-63.
- Barnes, R. O., Gieskes, J. M., Horvath, J., and Akiyama, W., 1979. Interstitial water studies, Legs 47A, B. In Sibuet, J. C., Ryan, W.B.F., et al., *Init. Repts. DSDP*, 47 (Pt. 2): Washington (U.S. Govt. Printing Office), 577-581.
- Beck, K. C., Blanc, G., Mascle, A., Moore, J. C., Taylor, E., Andreieff, P., Alvarez, F., Barnes, R., Behrmann, J., Brown, K., Clark, M., Dolan, J., Fisher, A., Gieskes, J., Hounslow, M., McLellan, P., Moran, K., Ogawa, Y., Sakai, T., Schoonmaker, J., Vrolijk, P., Wilkens, R., and Williams, C., 1988. Anatomie et Physiologie d'un prisme d'accrétion: premier résultats des forages du complexe de la ride de la Barbade Leg 110 ODP. *Bull. Soc. Géol. France*, 4:129-140.
- Biju-Duval, B., Moore, J. C., Moore, J. C., Taylor, E., Andreieff, P., Alvarez, F., Barnes, R., Behrmann, J., Brown, K., Clark, M., Dolan, J., Fisher, A., Gieskes, J., Hounslow, M., McLellan, P., Moran, K., Ogawa, Y., Sakai, T., Schoonmaker, J., Vrolijk, P., Wilkens, R., and Williams, C., 1984. *Init. Repts. DSDP*, 78A: Washington (U.S. Govt. Printing Office).
- Blanc, G., Gieskes, J., Mascle, A., et al., 1988. Advection des fluides interstitiels dans les séries sédimentaires du complexe d'accrétion de la Barbade (Leg 110 ODP). *Bull. Soc. Géol. France*, 4:453-460.
- Bray, C. J., and Karig, D. E., 1985. Porosity of sediments in accretionary prisms and some implications for dewatering processes. *J. Geophys. Res.*, 90:768-778.
- Coplen, T. B., and Hanshaw, B. B., 1973. Ultrafiltration by a compacted clay membrane. I. Oxygen and hydrogen isotopic fractionation. *Geochim. Cosmochim. Acta*, 37:2295-2310.
- DePaolo, D. J., and Ingram, B. L., 1985. High-resolution stratigraphy with strontium isotopes. *Science*, 227:938-940.
- Gieskes, J. M., 1974. Interstitial water studies, Leg 25. In Simpson, E.S.W., Schlich, R., et al., *Init. Repts. DSDP*, 25: Washington (U.S. Govt. Printing Office), 361-394.
- _____, 1983. The chemistry of interstitial waters of deep sea sediments: interpretation of Deep Sea Drilling data. In Riley, J. P., Chester, R. (Eds.), *Chemical Oceanography* (Vol. 8): London (Academic Press), 221-269.

- Gieskes, J. M., and Lawrence, J. R., 1981. Alteration of volcanic matter in deep sea sediments: evidence from the chemical composition of interstitial waters from deep sea drilling cores. *Geochim. Cosmochim. Acta*, 45:1687-1703.
- Gieskes, J. M., Elderfield, H., Lawrence, J. R., and LaKind, J., 1984. Interstitial water studies, Leg 78A. In Biju-Duval, B., Moore, J. C., et al., *Init. Repts. DSDP*, 78A: Washington (U.S. Govt. Printing Office), 377-384.
- Gieskes, J. M., Johnston, K., and Boehm, M., 1985. Appendix. Interstitial water studies, Leg 66. In von Huene, R., Aubouin, J., et al., *Init. Repts. DSDP*, 84: Washington (U.S. Govt. Printing Office), 961-967.
- Gieskes, J. M., Elderfield, H., and Palmer, M. R., 1986. Strontium and its isotopic composition in interstitial waters of marine carbonate sediments. *Earth Planet. Sci. Lett.*, 77:229-235.
- Gieskes, J. M., Lawrence, J. R., Perry, E. A., Grady, S. J., and Elderfield, H., 1987. Chemistry of interstitial waters and sediments in the Norwegian-Greenland Sea. *Chem. Geol.*, 63:143-155.
- Gieskes, J. M., and Peretsman, G., 1986. Water-chemistry procedures aboard JOIDES RESOLUTION: some comments. *Ocean Drilling Program, Technical Note No. 5*, 46.
- Hanshaw, B. B., and Coplen, T. B., 1973. Ultrafiltration by a compacted clay membrane. II. Sodium ion exclusion at various ionic strengths. *Geochim. Cosmochim. Acta*, 37:2311-2327.
- Harrison, W. E., Hesse, R., and Gieskes, J. M., 1982. Relationship between sedimentary facies and interstitial water chemistry of slope, trench, and Cocos Plate sites from the Middle America Trench Transect, DSDP Leg 67. In Aubouin, J., von Huene, R., et al., *Init. Repts. DSDP*, 67: Washington (U.S. Govt. Printing Office), 603-614.
- Hess, J., Bender, M. L., and Schilling, J. G., 1986. Evolution of the ratio of strontium-87 to strontium-86 in seawater from Cretaceous to Present. *Science*, 231:979-984.
- Hesse, R., Lebel, J., and Gieskes, J. M., 1985. Interstitial water chemistry of gas hydrate bearing sections on the Middle America Trend slope, DSDP Leg 84. In von Huene, R., Aubouin, J., et al., *Init. Repts. DSDP*, 84: Washington (U.S. Govt. Printing Office), 727-737.
- Jenden, P., and Gieskes, J. M., 1983. Chemical and isotopic composition of interstitial water from Deep Sea Drilling Project Sites 533 and 534. In Sheridan, R. E., Gradstein, F. M., et al., *Init. Repts. DSDP*, 76: Washington (U.S. Govt. Printing Office), 453-461.
- Kharaka, Y. K., and Berry, F. A., 1973. Simultaneous flow of water and solute through geological membranes. I: experimental investigations. *Geochim. Cosmochim. Acta*, 49:761-768.
- Lawrence, J. R., and Gieskes, J. M., 1981. Constraints on water transport and alteration in the oceanic crust from the isotopic composition of pore water. *J. Geophys. Res.*, 86:7924-7934.
- Manheim, F. T., 1966. A hydraulic squeezer for obtaining interstitial waters from consolidated and unconsolidated sediments. *U.S. Geol. Surv. Prof. Pap.*, 550-C:256.
- _____, 1974. Comparative studies on extraction of sediment interstitial waters: discussion and comment on the current state of interstitial water studies. *Clays Clay Miner.*, 22:337.
- Manheim, F. T., and Sayles, F. L., 1974. Composition and origin of interstitial waters of marine sediments, based on deep sea drill cores. In Goldberg, E. D. (Ed.), *The Sea* (Vol. 5): New York (Wiley-Interscience):527-568.
- Marine, I. W., and Fritz, S. J., 1981. Osmotic model to explain anomalous hydraulic heads. *Water Resour. Res.*, 17:3-82.
- Masclé, A., Moore, J. C., et al. 1988. *Proc. ODP, Init. Repts.*, 110: College Station, TX (Ocean Drilling Program).
- McDuff, R. E., 1981. Major cation gradients in DSDP interstitial waters: the role of diffusive exchange between seawater and the upper ocean crust. *Geochim. Cosmochim. Acta*, 45:1701-1715.
- McDuff, R. E., and Gieskes, J. M., 1976. Calcium and magnesium profiles in DSDP interstitial waters: diffusion or reaction? *Earth Planet. Sci. Lett.*, 33:1-10.
- Moore, J. C., and Gieskes, J. M., 1980. Interaction between sediment and interstitial water near the Japan Trench, Leg 57, DSDP. In Langseth, M., Okada, H., et al., *Init. Repts. DSDP*, 57 (Pt. 2): 1269-1275.
- Moore, J. C., Masclé, A., Taylor, E., Alvarez, F., Andreieff, P., Barnes, R., Beck, C., Behrmann, J., Blanc, G., Brown, K., Clark, M., Dolan, J., Fisher, A., Gieskes, J., Hounslow, M., McClellan, P., Moran, K., Ogawa, Y., Sakai, T., Schoonmaker, J., Vrolijk, P. J., Wilkens, R., Williams, C., 1987. Expulsion of fluids from depth along a subduction-zone décollement horizon. *Nature*, 326:785-788.
- Palmer, M. R., and Elderfield, H., 1985. The Sr isotopic composition of seawater over the past 75 million years. *Nature*, 314:526-528.
- Presley, B. J., 1971. Techniques for analyzing interstitial water samples. Part 1: determination of minor and major inorganic constituents. In Winterer, E. L., Riedel, W. R., et al., *Init. Repts. DSDP*, 7 (Pt. 2): Washington (U.S. Govt. Printing Office), 1749-1755.
- Sayles, F. L., 1970. Preliminary geochemistry. In Bader, R. G., Gerard, R. D., et al., *Init. Repts. DSDP*, 4: Washington (U.S. Govt. Printing Office), 645-655.
- Shipboard Scientific Party, 1988. Synthesis of shipboard results: Leg 110 transect at the northern Barbados Ridge. In Masclé, A., Moore, J. C., et al., *Proc. ODP, Init. Repts.*, 110: College Station, TX (Ocean Drilling Program), 577-591.
- Shiskina, O. V., 1966. Metody issledovaniya mors kikh i okenicheskikh olovnykh vod (methods of studying marine and oceanic pore fluids), Porvyy rastvory i metody izucheniya, Nauka i Technika, Minsk, 167-177.
- Wang, Y. C., and Gieskes, J. M., 1988. Halide distributions in Deep Sea Drilling interstitial waters: some observations and problems. *Eos*, 69:1263.

Date of initial receipt: 13 December 1988

Date of acceptance: 8 May 1989

Ms 110B-170

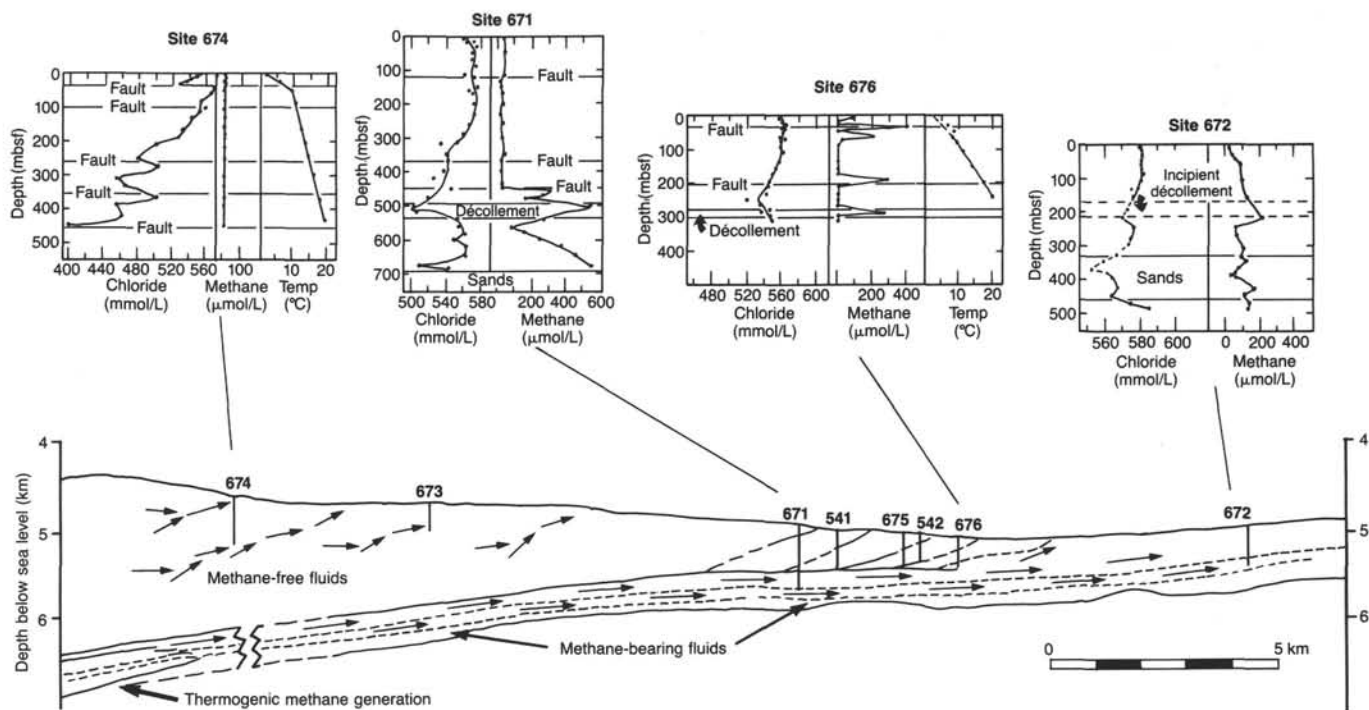


Figure 22. Suggested path of fluid migration in Northern Barbados accretionary complex.